OPEN ACCESS Freely available online

PLoS one

Real-Time Imaging of Rabbit Retina with Retinal Degeneration by Using Spectral-Domain Optical Coherence Tomography

Yuki Muraoka[1], Hanako Ohashi Ikeda[1]*, Noriko Nakano[1], Masanori Hangai[1], Yoshinobu Toda[2], Keiko Okamoto-Furuta[2], Haruyasu Kohda[2], Mineo Kondo[3], Hiroko Terasaki[4], Akira Kakizuka[5], Nagahisa Yoshimura[1]

1 Department of Ophthalmology and Visual Sciences, Kyoto University Graduate School of Medicine, Kyoto, Japan, **2** Center for Anatomical Studies, Kyoto University Graduate School of Medicine, Kyoto, Japan, **3** Department of Ophthalmology, Mie University School of Medicine, Tsu, Japan, **4** Department of Ophthalmology, Nagoya University Graduate School of Medicine, Nagoya, Japan, **5** Laboratory of Functional Biology, Kyoto University Graduate School of Biostudies and Solution Oriented Research for Science and Technology, Kyoto, Japan

Abstract

Background: Recently, a transgenic rabbit with rhodopsin Pro 347 Leu mutation was generated as a model of retinitis pigmentosa (RP), which is characterized by a gradual loss of vision due to photoreceptor degeneration. The purpose of the current study is to noninvasively visualize and assess time-dependent changes in the retinal structures of a rabbit model of retinal degeneration by using speckle noise-reduced spectral-domain optical coherence tomography (SD-OCT).

Methodology/Principal Findings: Wild type (WT) and RP rabbits (aged 4–20 weeks) were investigated using SD-OCT. The total retinal thickness in RP rabbits decreased with age. The thickness of the outer nuclear layer (ONL) and between the external limiting membrane and Bruch's membrane (ELM–BM) were reduced in RP rabbits around the visual streak, compared to WT rabbits even at 4 weeks of age, and the differences increased with age. However, inner nuclear layer (INL) thickness in RP rabbits did not differ from that of WT during the observation period. The ganglion cell complex (GCC) thickness in RP rabbits increased near the optic nerve head but not around the visual streak in the later stages of the observation period. Hyper-reflective change was widely observed in the inner segments (IS) and outer segments (OS) of the photoreceptors in the OCT images of RP rabbits. Ultrastructural findings in RP retinas included the appearance of small rhodopsin-containing vesicles scattered in the extracellular space around the photoreceptors.

Conclusions/Significance: In the current study, SD-OCT provided the pattern of photoreceptor degeneration in RP rabbits and the longitudinal changes in each retinal layer through the evaluation of identical areas over time. The time-dependent changes in the retinal structure of RP rabbits showed regional and time-stage variations. *In vivo* imaging of RP rabbit retinas by using SD-OCT is a powerful method for characterizing disease dynamics and for assessing the therapeutic effects of experimental interventions.

Citation: Muraoka Y, Ikeda HO, Nakano N, Hangai M, Toda Y, et al. (2012) Real-Time Imaging of Rabbit Retina with Retinal Degeneration by Using Spectral-Domain Optical Coherence Tomography. PLoS ONE 7(4): e36135. doi:10.1371/journal.pone.0036135

Editor: Steven Barnes, Dalhousie University, Canada

Received November 27, 2011; **Accepted** March 26, 2012; **Published** April 27, 2012

Funding: This research was supported by Research grants from the Astellas Foundation for Research on Metabolic Disorders and the Japan Foundation for Applied Enzymology, and a Grant-in-Aid for Young Scientists (22791656) from the Ministry of Education, Culture, Sports, Science and Technology (MEXT). The funders had no role in study design, data collection and analysis, decision to publish, or preparation of the manuscript.

Competing Interests: The authors have declared that no competing interests exist.

* E-mail: hanakoi@kuhp.kyoto-u.ac.jp

Introduction

Retinitis pigmentosa (RP) is an inherited retinal disorder characterized by a progressive loss of visual function due to degeneration of rod and cone photoreceptors and eventual atrophy of the entire retina [1,2]. However, there are no effective treatments for RP. Various animal models of RP have been developed and studied to elucidate the pathophysiology of the disease and to develop new treatments [3–10]. Of these models, only monkeys have a macula, an important area for vision due to the high density of cone photoreceptors. However, it is not easy to study the pathophysiology of RP in monkeys due to handling and breeding difficulties. Rabbits are known to have a visual streak, where the rod and cone photoreceptor density is highest, about 3 mm ventral to the optic nerve head (ONH) [11,12]. Rabbits are easy to breed and handle, and the physiology and morphology of rabbit retina is well understood [11–14]. Additionally, in mid-sized animals like rabbits, surgical treatments such as subretinal injection of cells for regenerative therapy [15,16], vectors for gene therapy [17], and implantation of intraocular devices [18,19] are easily performed. Therefore, rabbits are very useful for studying retinal diseases and testing new therapeutic interventions. For these reasons, we used transgenic (Tg) rabbits with mutated rhodopsin (Pro 347 Leu, RP rabbits) as a mid-sized model for RP

[20] to study the pathophysiology and develop new evaluation systems for retinal degeneration.

Optical coherence tomography (OCT) devices allow non-invasive detection of retinal architecture, including quantitative measurements of retinal thickness and longitudinal observation of the retinal architecture [21]. The technological advances in spectral-domain OCT (SD-OCT) have enabled high-speed scanning and improved image resolution [22]. Furthermore, the exact averaging of B-scans with a three-dimensional eye-tracking system and high-speed scanning have enabled sufficient reduction in speckle noise, the most influential artificial noise that blurs the boundaries between retinal layers [23,24]. These advances have improved visualization of individual retinal layers, including both the outer retina and the inner retina (i.e., ganglion cell layer and inner plexiform layer [IPL] in humans) [25,26]. SD-OCT imaging also enables evaluation of the junction between the inner segment (IS) and the outer segment (OS) of the photoreceptors (IS/OS) [27–29] and that of the external limiting membrane (ELM) [30,31] as hallmarks of photoreceptor integrity. That is, visual function can be speculated from OCT images to some extent. Thus, the use of OCT imaging in humans has contributed to a more detailed understanding of the pathophysiology of many retinal diseases. In mice, the retina has been clearly visualized using SD-OCT [32–37]. Thus, in experimental animals, SD-OCT may allow *in vivo* detection and monitoring of changes in retinal architecture without sacrificing animals.

In mouse models of retinal degeneration, Fischer [36] and Huber et al. [32] detected and analyzed photoreceptor degeneration by using SD-OCT. They imaged the thinning of inner retinal layers and compared the total retinal thickness with that of normal mice in several mouse RP models. Yamauchi et al. reported the retinal architecture of rabbits by using SD-OCT following iodoacetic acid-induced photoreceptor degeneration [38]. However, retinal pathomorphology of genetically engineered rabbit models of RP, which mimic human RP [20], and longitudinal assessment of changes in the individual retinas remain to be studied with SD-OCT.

The purpose of this study was to visualize the time-dependent changes in photoreceptors, elucidate the pattern of changes in each retinal layer around the visual streak in identical eyes of RP rabbits by using SD-OCT, and assess the visual functions by electroretinography (ERG).

Results

Visualization of retinal structures in RP rabbits with SD-OCT

We first investigated whether the retinal structures of WT rabbits could be clearly visualized using SD-OCT. Vertical OCT images, which passed through the center of the ONH (Fig. 1A), permitted clear identification of each retinal layer, the choroid, and sclera of WT rabbits (Figs. 1B and 1C). The ELM and IS/OS lines were also clearly identifiable, the integrity of which have been shown to be positively associated with visual function. In the vertical OCT images, the scleral ring was defined as the edge of the ONH so that OCT measurements could be longitudinally compared between each rabbit and between WT and RP rabbits (Fig. 1B).

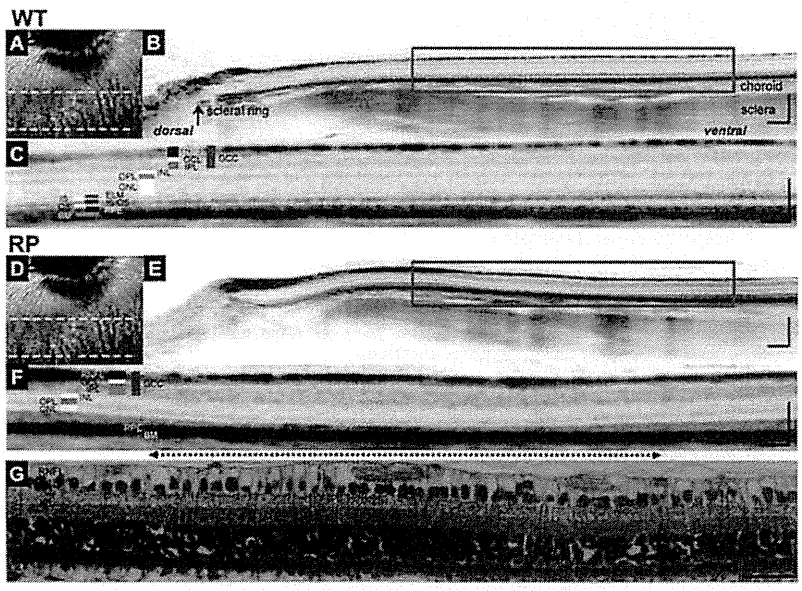

Figure 1. SD-OCT images of WT and Retinitis Pigmentosa (RP) rabbit retinas and histology of the visual streak in an RP rabbit. (A) A fundus infrared image of a WT rabbit retina, including optic nerve head (ONH) and visual streak. The area between dotted lines is the visual streak. (B) A vertical SD-OCT image along the green arrow in panel A, which passes through the center of the ONH. On this vertical image, the scleral ring was regarded as the lower margin of the ONH. (C) A magnified OCT image of the area enclosed by the blue square in panel B, which includes the visual streak. (D) A fundus infrared image of a RP rabbit retina, including the ONH and visual streak. (E) A vertical SD-OCT image of a 20-week-old RP rabbit along the green arrow in panel D. (F) A magnified OCT image of the area enclosed by the blue square in panel E. The 2.2 mm width of this OCT section was vertically cut between 1.8 mm and 4.0 mm ventral to the inferior edge of the ONH. A dotted arrow indicates the region of the visual streak. (G) Hematoxylin-Eosin staining of a retinal section corresponding to the area in the OCT image in F. Scale Bar = 200 μm (B, E), 100 μm (C, F), and 50 μm (G). RNFL, retinal nerve fiber layer; GCL, ganglion cell layer; IPL, inner plexiform layer; GCC, ganglion cell complex; INL, inner nuclear layer; OPL, outer plexiform layer; ONL, outer nuclear layer; ELM, external limiting membrane; IS, inner segments of photoreceptors; OS, outer segments of photoreceptors; IS/OS, junctions between IS and OS; RPE, retinal pigment epithelium; and BM, Bruch's membrane.
doi:10.1371/journal.pone.0036135.g001

Next, we examined a 20-week-old RP rabbit that expressed mutated rhodopsin (Figs. 1D–1F). The outer nuclear layer (ONL) of the RP rabbit was much thinner than the WT rabbit. Furthermore, in the RP rabbit, the photoreceptors around the visual streak (indicated by the dotted arrow), where the densities of rod and cone photoreceptors were the highest, appeared to be more severely damaged than in any other area. In this area, the ONL was very thin and the outer plexiform layer (OPL) was faint or absent depending on the distance from the ONH and the IS/OS line was undetectable (Fig. 1F). This regional variation in photoreceptor damage was also detected with hematoxylin and eosin (H&E) staining in the same eye (Fig. 1G).

Time-dependent changes in the photoreceptor layers and in the visual function of RP rabbits

As observations revealed that photoreceptor damage was severe around the visual streak, we were encouraged to investigate the time-dependent changes in the photoreceptors of identical RP rabbits beneath the visual streak with SD-OCT and compared them with those of the WT rabbits (Fig. 2A). At 4 weeks of age (with the youngest that can be examined by OCT), the ONL of RP rabbits was almost as thick as WT rabbits. Following 4 weeks of age, the ONL thickness in RP rabbits decreased. At 20 weeks, the ONL thickness in RP rabbits was much smaller than in WT rabbits. Photoreceptor IS and OS, where visual phototransduction occurs, were thin in RP rabbits. In contrast, the architecture of the inner retina was relatively preserved in RP rabbits at both 10 and 20 weeks of age.

In the current SD-OCT study, there were additional findings in the photoreceptor layers. In the sections of WT rabbits, the reflectivity of IS and OS was low compared to that of the ELM and IS/OS lines. In contrast, the IS and OS were highly reflective in RP rabbits, and almost equivalent to the ELM and IS/OS lines throughout the study ages (Fig. 2A).

To compare the SD-OCT data with those from the histological examination, histological sections of the age-matched RP and WT rabbits were prepared (Fig. 2B). The number of photoreceptors and thickness of the ONL, IS, and OS in the RP rabbits decreased with age, which is consistent with those of a previous report [20]. At 20 weeks of age, the nuclei of photoreceptors in RP rabbits were reduced to 1 or 2 rows, which was much less compared to WT rabbits. The magnitude of the decrease in ONL thickness appears similar between the histological and SD-OCT data (Figs. 2A and 2B). In the histological sections of a 4-week-old RP rabbit, the total retinal thickness and the ONL thickness were almost the same as those of the WT rabbit, and the IS and OS appeared intact. The high reflectivity in the IS and OS observed in the OCT sections was difficult to explain by the histological sections (Figs. 2A and 2B).

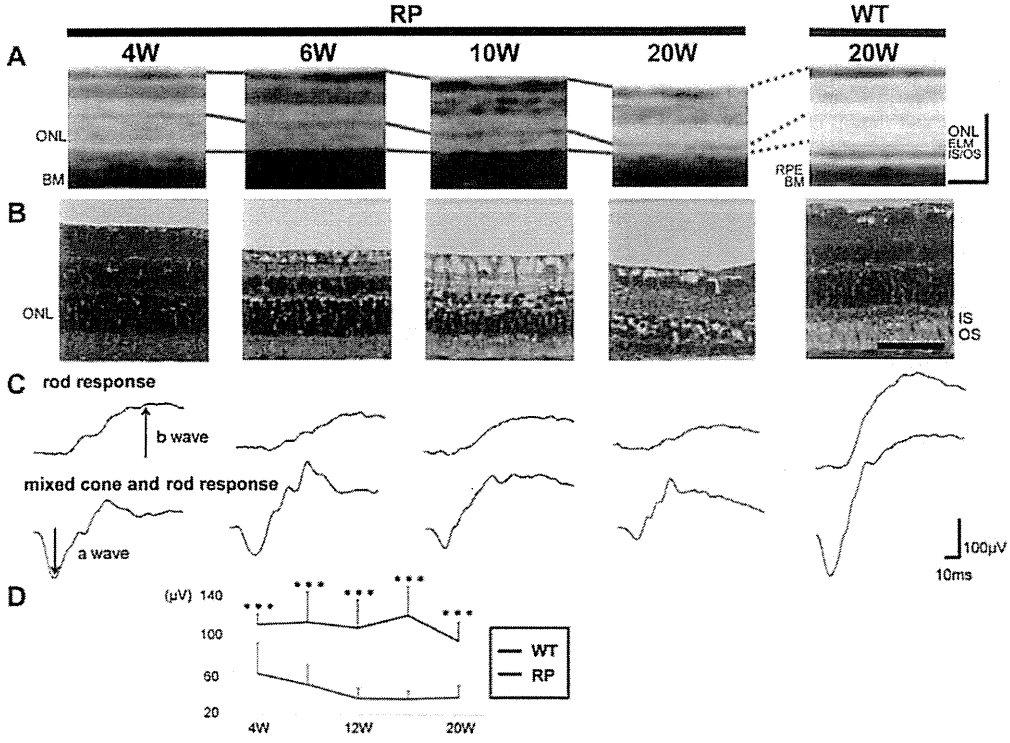

Figure 2. Time-dependent changes in morphological features of the retina and visual function in the RP rabbits. (A) SD-OCT images beneath the visual streak in an RP rabbit at 4, 6, 10, and 20 weeks and in a 20-week-old WT rabbit. The total retinal and ONL thickness in the RP rabbits decreased with age. The IS and OS were highly reflective in the RP rabbits compared with the WT rabbits. ONL, outer nuclear layer; and OS, outer segments of photoreceptors. (B) Hematoxylin-eosin staining of retinas in 4-, 6-, 10-, and 20-week-old RP and 20-week-old WT rabbits. The ONL in RP rabbits thinned with age. In 20-week-old RP rabbits, only 1–2 layers of nuclei were detected in the ONL. (C) Representative scotopic electroretinograms of 4-, 6-, 10-, and 20-week-old RP and 20-week-old WT rabbits. (D) The a-wave amplitude of the mixed rod and cone response. The amplitude was smaller in the RP rabbits than in the WT rabbits. The differences between the WT and RP rabbits were significant at all study points between 4 and 20 weeks. *$P<0.05$, ***$P<0.001$ (unpaired t-test). Scale Bar = 100 μm in A, and 50 μm in B. ONL, outer nuclear layer; ELM, external limiting membrane; IS/OS, junctions between inner segment (IS) and outer segment (OS); RPE, retinal pigment epithelium; and BM, Bruch's membrane.

doi:10.1371/journal.pone.0036135.g002

Next, to evaluate visual function of the rod and cone systems of RP rabbits, scotopic full-field ERG was recorded (Fig. 2C). The a-wave of the mixed cone and rod response, which mainly originates from the photoreceptors, was smaller in RP rabbits (61.2±30.5 μV) (mean ± SD) than in WT rabbits (110.3±10.7 μV; $P=0.010$, unpaired *t*-test) as early as 4 weeks. The a-wave amplitude was reduced with RP rabbit aged (Fig. 2D). At the age of 20 weeks, the a-wave amplitude decreased to 37.6±11.5 μV in RP rabbits and was significantly less than that of WT rabbits (93.5±19.0 μV; $P<0.001$, unpaired *t*-test, Figs. 2C and 2D). The b-wave amplitude of the rod response, which originates indirectly from bipolar and Müller cells, was 97.3±33.2 μV in RP rabbits and was less than that of WT rabbits (280.8±71.3 μV; $P<0.001$, unpaired *t*-test, Fig. 2C). These data suggest that the visual function of both the rod and cone systems was disturbed in RP rabbits, consistent with a previous report [20]. These results indicate that loss of photoreceptors and concomitant visual dysfunction gradually occurs in RP rabbits.

Vesicles cleaved from photoreceptors and disorganization of IS and OS in RP rabbits account for the hyper-reflectivity seen in SD-OCT images

To elucidate the cause of the hyper-reflective change in the outer photoreceptor layers of RP rabbits in SD-OCT sections, we examined and compared the ultrastructure of the retina between RP and WT rabbits at 4 or 20 weeks of age. In WT rabbits, the IS and OS exhibited a dense and regular arrangement (Figs. 3A, 3B, S1A and S1B). In contrast, in the RP retinas, the IS and OS were less organized at 4 weeks of age (Figs. 3C and 3D), and they were mostly absent at 20 weeks of age (Figs. S1C and S1D). Magnified images of the RP retinas revealed large number of small, approximately 100 nm, vesicles scattered in the extracellular space around the photoreceptors (arrowheads in Fig. 3D and S1D). These small vesicles appeared to be cleaved from the membrane of the IS in RP rabbits (arrows in Fig. 3E and S1D).The disrupted organization and the presence of vesicles between the IS and OS on ultra microscopy may account for the hyper-reflectivity seen in the corresponding area of the SD-OCT images.

To determine the origin of the vesicles, we performed ultrastructural immunohistochemistry by using monoclonal antibodies against rhodopsin (Fig. 3F). In RP retinas, numerous vesicles with dots were observed, indicating the presence of rhodopsin within the vesicles (disintermediated arrowheads in Fig. 3F).

Time-dependent changes in the individual retinal layers in SD-OCT sections exhibit regional and time-stage variations in RP rabbits

In the SD-OCT examinations, the retinal thickness in the RP rabbits appeared to decrease with age. Therefore, we quantitatively measured the mean total retinal thickness around the visual streak in the WT and RP rabbits (Figs. 4A and S2). As shown in Fig. 4A, the total retinal thickness in WT rabbits did not change with age, whereas that of the RP rabbits progressively decreased. The total retinal thickness in WT and RP rabbits was not significantly different at 4 weeks. However, after 6 weeks, the differences in the total retinal thickness increased and continued with age. At 20 weeks, the total retinal thickness in RP rabbits was 165.8±8.5 μm and significantly smaller than that of WT rabbits (194.3±7.7 μm; $P<0.001$, unpaired *t*-test).

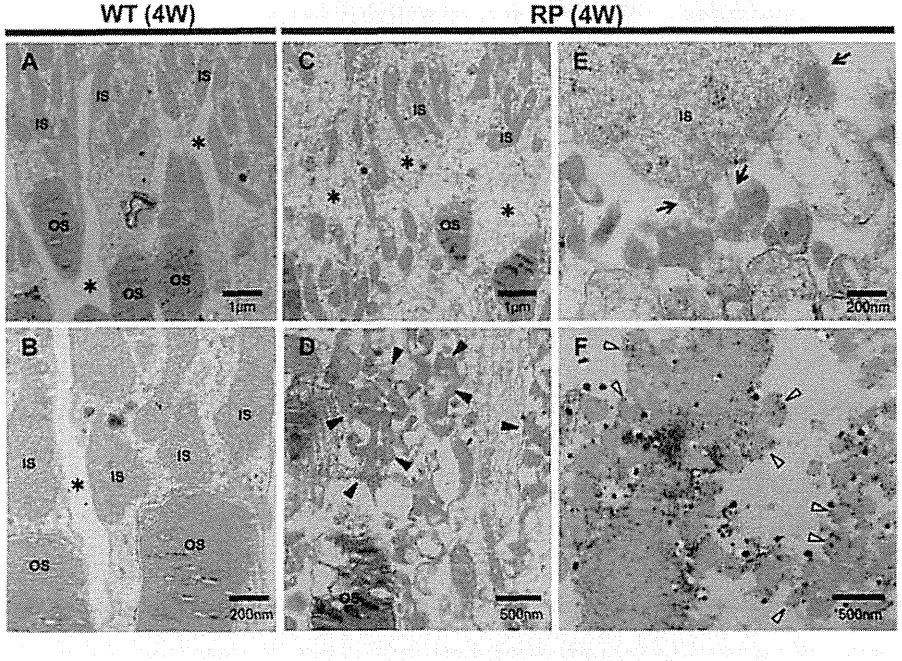

Figure 3. Ultrastructure of photoreceptors in WT and RP rabbits. (A, B) Ultrastructure of photoreceptors in 4-week-old WT rabbits. The inner (IS) and outer segments (OS) of the photoreceptors were regular and dense. There are no vesicles in the extracellular spaces (*). (C–E) Ultrastructure of the photoreceptors in the 4-week-old RP rabbits. The IS and OS were less organized than those in the WT rabbits. In the magnified image (D), the RP rabbit retina showing many small vesicles (arrowheads) accumulated in the extracellular spaces (indicated with * in panel C). The vesicles appeared to be cleaved from the IS into the extracellular space around the photoreceptors (arrows in panel E). (F) Ultrastructural immunohistochemistry by using an anti-rhodopsin antibody. The small vesicles (disintermediated arrowheads) in the extracellular spaces around the photoreceptors exhibit black dots indicating the presence of rhodopsin.
doi:10.1371/journal.pone.0036135.g003

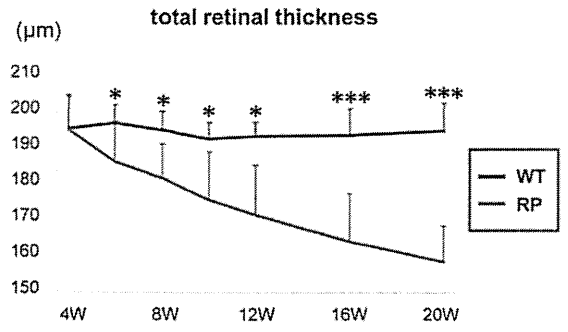

Figure 4. Time-dependent changes in total retinal thickness, and mixed cone and rod response in the WT and RP rabbits. The total retinal thicknesswas measured within a circle 1 mm in diameter 3 mm ventral to the lower margin of the ONH and averaged. The total retinal thickness in the WT rabbits (indicated with a blue line) was unchanged during observation, whereas that in the RP rabbits (indicated with a red line) severely decreased with age. *$P<0.05$, ***$P<0.001$ (unpaired t-test).
doi:10.1371/journal.pone.0036135.g004

OCT examination showed that the photoreceptors were most severely damaged at the visual streak, approximately 3 mm ventral to the ONH [11]. Therefore, we longitudinally examined regional and periodical variations in the progression of retinal degeneration in RP rabbits. For this purpose, we measured the thickness of each retinal layer within 0.5-mm areas 4 mm ventral to the lower edge of the ONH as a function of distance from the lower optic disc margin at 4, 6, 10, and 20 weeks by using the vertical OCT images that passed through the center of the ONH and visual streaks (Fig. S3).

ONL thickness. We first evaluated the thickness of the ONL where the nuclei of photoreceptors are located (Fig. 5A). In WT rabbits, the ONL in each area became slightly thinner with age. In younger WT rabbits (4–6 weeks old), the ONL was thinner in areas more distant from the ONH. In RP rabbits, the decrease in ONL thickness with age was more progressive than that of WT rabbits. At any age examined, thinning of the ONL was greater in areas more distant from the ONH. At 10 and 20 weeks, the ONL was thinnest in the area 3.0–3.5 mm ventral to the ONH.

At 4 weeks, the ONL thickness in RP rabbits was significantly less than that of WT rabbits in only the area 3.0–3.5 mm from the ONH ($P=0.037$, unpaired t-test). Areas that exhibited a difference in ONL thickness between WT and RP rabbits expanded with age. At 20 weeks, the ONL thickness in RP rabbits was significantly smaller than that of WT rabbits in each of the 7 areas examined ($P<0.001$, unpaired t-test, Fig. 5E).

ELM–BM thickness. The ELM–BM thickness was evaluated because the area between the ELM and BM includes the length of the IS and OS where visual phototransduction occurs (Figs. 5B and S3). In WT rabbits, the ELM–BM thickness was larger in areas more distant from the ONH at any age examined. On the other hand, in RP rabbits, the differences in the ELM–BM thickness between areas as a function of distance from the ONH were smaller compared to those of WT rabbits at 4–10 weeks; the ELM–BM thickness appeared to decrease mainly in the areas distant from the optic disc. In 20-week-old RP rabbits, the ELM–BM thickness markedly decreased in the area 2.5–3.5 mm ventral to the ONH and was significantly less than that in the corresponding areas in WT rabbits ($P<0.001$, unpaired t-test, Fig. 5E).

INL thickness. The INL comprises the nuclei of bipolar, horizontal, amacrine, and Müller cells. The INL thickness was larger in areas more distant from the ONH in both WT and RP rabbits at the ages of 4 to 20 weeks (Fig. 5C). The INL thickness in WT and RP rabbits was not significantly different in each corresponding area at all the ages examined (Fig. 5E).

GCC thickness. The GCC consists of the retinal nerve fiber layer (axons of ganglion cells), ganglion cell layer (somas of ganglion cells), and IPL. To determine the influence of photoreceptor degeneration on the inner retina, GCC thickness was measured (Figs. S3 and 5D). The GCC thickness in the WT and RP rabbits exhibited a similar pattern in all the areas examined at the ages of 4 and 6 weeks. However, in 20-week-old RP rabbits, the GCC thickness in the areas close to the ONH was larger than in younger RP rabbits and in the corresponding areas of 20-week-old WT rabbits ($P<0.001$ for both, unpaired t-test, Fig. 5E).

In summary, the decrease in the ONL and ELM–BM thickness in RP rabbits was first detected in the areas approximately 3.0 mm ventral to the lower edge of the ONH (areas corresponding to the visual streak). Thinning of the IS and OS (measured as the ELM–BM thickness) followed thinning of the ONL. In contrast, the INL thickness in RP rabbits did not change throughout the observational period of 4 to 20 weeks. The GCC thickness in RP rabbits increased in areas away from the visual streaks but close to the ONH in the later phase of observation (Fig. 5E).

Discussion

In this study, we examined time-dependent changes in photoreceptor degeneration in identical RP rabbits, and compared the pattern of changes in individual retinal layers between WT and RP rabbits for the first time by using SD-OCT. In RP rabbits, we observed regional differences in the degree of photoreceptor loss. That is, the ONL (ONL: the somas of photoreceptors) in RP rabbits was thinnest beneath the visual streak, where the densities of rod and cone photoreceptors were the highest in WT rabbits, and the photoreceptors of RP rabbits were relatively preserved in the area near the ONH. The current observations by using SD-OCT revealed longitudinal changes in the RP rabbit retina that were fairly consistent with a previous histological study of the RP rabbits [20] and reports based on other animal models of RP [3,9].

To elucidate the unique "highly reflective IS and OS" feature of the outer photoreceptor layer during photoreceptor degeneration in RP rabbits, an electron microscopy study was conducted on 4- or 20-week-old RP rabbits. We detected vesicles around the photoreceptors and loss of most of the IS and OS. We speculate that these destructive structures in RP rabbits cause the hyper-reflectivity seen in the outer photoreceptor layers (between ELM and BM) on SD-OCT images (Fig. 2A).The vesicles appeared to be cleaved from the IS, as described in a previous report [20]. Moreover, these vesicles were shown to include rhodopsin by ultrastructural immunohistochemistry (Fig. 3F), indicating that the particles were derived from photoreceptors. In SD-OCT images of 4-week-old RP rabbits, the area between the ELM and BM was hyper-reflective even though the reflectivity and the thickness of the ONL were unchanged (Fig. 2A). These observations point to the mechanism by which photoreceptors degenerate in RP rabbits. That is, defective transport of rhodopsin from the IS to the OS, which was demonstrated in mice with mutated rhodopsin P347S by using an antibody against the mutated rhodopsin [39], is followed by cleavage of vesicles from the IS, and finally cell bodies of photoreceptors degenerate. It is speculated that early stage RP patients may have mutations in the rhodopsin gene if hyper-reflective patterns are detected with SD-OCT in the area corresponding to the IS and OS, though further studies are needed to confirm this speculation.

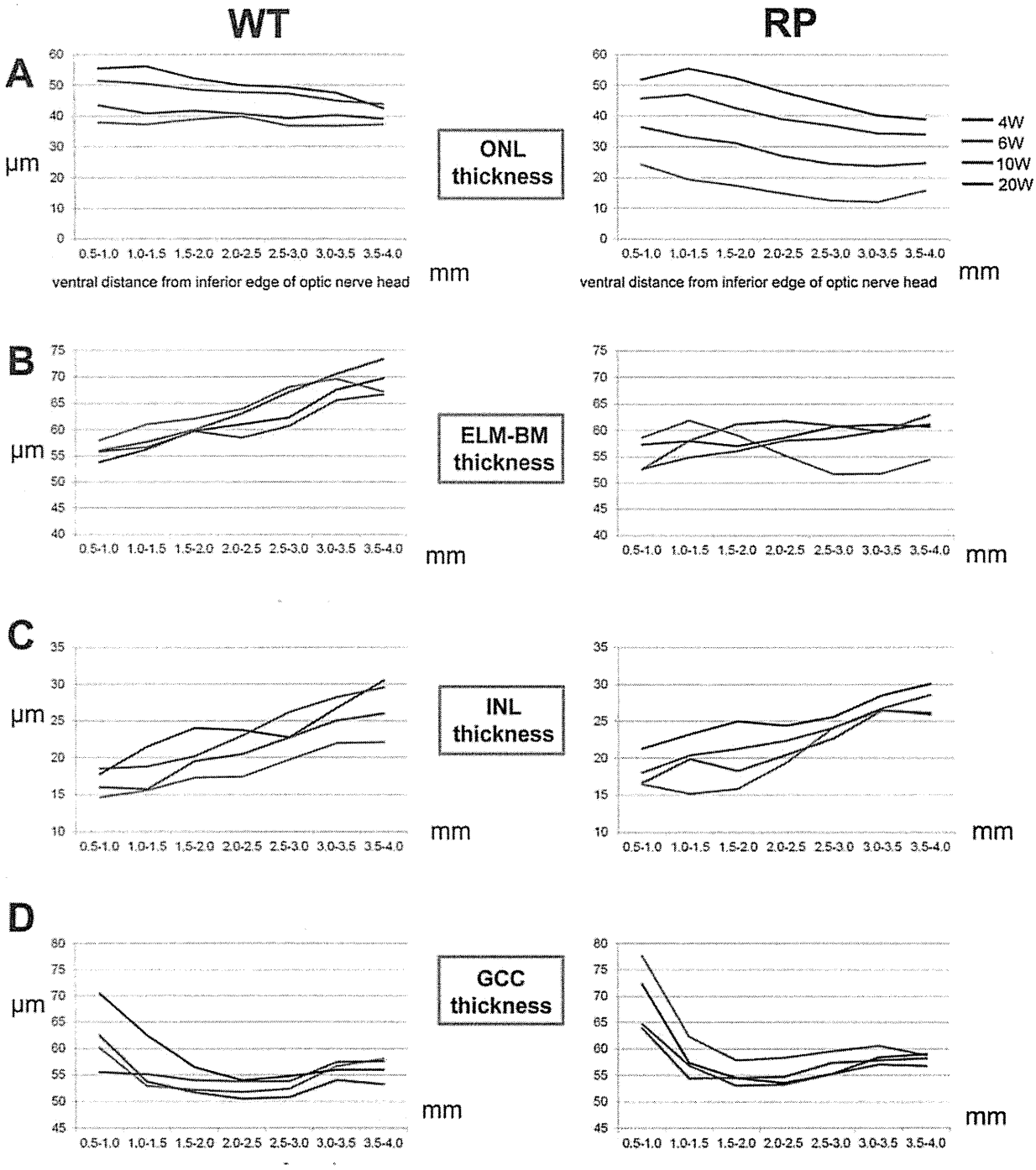
WT
RP
A
ONL thickness
μm
mm
ventral distance from inferior edge of optic nerve head
4W
6W
10W
20W
B
ELM-BM thickness
C
INL thickness
D
GCC thickness
E
ONL
ELM-BM
INL
GCC
0.5-1.0 1.0-1.5 1.5-2.0 2.0-2.5 2.5-3.0 3.0-3.5 3.5-4.0

Figure 5. Time-dependent changes in the thickness of individual retinal layers in WT and RP rabbits. (A–D) Time-dependent changes in ONL (A), ELM–BM (B), INL (C), and GCC (D) thickness measured with vertical OCT sections of WT and RP rabbits. Mean values at 4, 6, 10, and 20 weeks are indicated with blue, red, green, and purple lines, respectively. X-axes indicate the distance from the inferior edge of the ONH. (E) A schema to show time course and regional variations in the thickness of each retinal layer in RP rabbits from 4 to 20 weeks. Blue color indicates the regions where retinal thickness of RP rabbits was significantly smaller than that of WT rabbits. Orange color indicates the regions where retinal thickness of RP rabbits was significantly larger than that of WT rabbits. Deep and light colors indicate $P<0.001$ and $P<0.05$, respectively (unpaired *t*-test). ONL, outer nuclear layer; ELM, external limiting membrane; BM, Bruch's membrane; INL, inner nuclear layer; and GCC, ganglion cell complex.
doi:10.1371/journal.pone.0036135.g005

Aleman et al. reported the following disease sequence in human and murine RP caused by mutation of the rhodopsin gene: ONL diminution with INL thickening, amalgamation of residual ONL with the thickened INL, and progressive retinal remodeling with eventual thinning seen in OCT [40]. In our SD-OCT study, the INL thickness was not significantly different between WT and RP rabbits at the ages of 4 to 20 weeks. In contrast, the GCC thickness in RP rabbits paradoxically increased in the later phase of observation. Previous studies have suggested that the increase in the INL/inner retinal thickness in patients with RP maybe related to Müller glial activation with hypertrophy [40–42]. In the current study with RP rabbits, the observational period may be too short to detect an increase in INL thickness, or the gliosis of Müller cells may occur preferably within the GCC than in the INL.

This study has some limitations. The area imaged with SD-OCT was quite restricted such that the degeneration in RP retinas obtained with SD-OCT did not always correlate with the total retinal function. Furthermore, OCT or ERG could not be performed on rabbits younger than 4 weeks as their eyelids had not yet opened.

In conclusion, despite these short comings, *in vivo* time-dependent changes in the retinal structures were seen layer-by-layer in RP rabbits by using SD-OCT. These changes in the retinal structure had regional and temporal variations not only in the outer retina but also in the inner retina of RP rabbits. This study demonstrates that *in vivo* imaging with SD-OCT can facilitate the characterization of morphological disease dynamics and serve as a powerful tool for developing new treatments, such as gene therapy, intraocular devices, and neuroprotective treatments, in rabbit models of RP.

Methods

Experimental animals

This study was conducted in accordance with the Association Research in Vision and Ophthalmology (ARVO) Statement for the Use of Animals in Ophthalmic and Vision Research. All the protocols were approved by the Institutional Review Board of the Kyoto University Graduate School of Medicine (MedKyo11229).

New Zealand White rabbits (NZW, WT) and RP rabbits with rhodopsin P347L mutation (NZW, RP) [20] were purchased from Kitayama Labes Co., Ltd (Ina, Nagano, Japan). All rabbits were kept under a 14 h–10 h light-dark cycle (approximately 200 lux), given free access to water, and fed once a day. For the ERG recording and SD-OCT image acquisition, male WT (n = 4–10 eyes) and RP rabbits (n = 10–16 eyes) were used.

Retinal histology

Rabbit eyes were fixed overnight in a mixture of 10% neutral buffered formalin and 2.5% glutaraldehyde and then transferred to 10% neutral buffered formalin. The tissues were trimmed, embedded in paraffin, sectioned vertically through the optic nerve (superior-inferior), and stained with hematoxylin and eosin. The retina beneath the visual streak was examined and compared between 10- and 20-week-old WT and RP rabbits.

ERG

ERG was performed to assess the visual function of WT and RP rabbits at 4, 6, 10, and 20 weeks. Pupils were dilated with tropicamide (0.5%) and phenylephrine (0.5%) eye drops. Rabbits were dark-adapted for more than 60 min before anesthetization with an intramuscular injection of ketamine (25 mg/kg) and xylazine (2 mg/kg). ERG was recorded using a gold loop corneal electrode with a light-emitting diode (Mayo Corp., Inazawa, Japan). A reference electrode was placed in the mouth, and a ground electrode was attached to the ear. Stimuli were produced with a light-emitting diode stimulator (Mayo Corp.). The ERG response signals were amplified, digitized at 10 kHz with a band-pass filter of 0.3 to 500 Hz and analyzed (PowerLab 2/25; AD instruments, New South Wales, Australia). Two steps of stimulus intensities (ISCEV standard; scotopic 0.01 and scotopic 3.0) were used for evaluating rod and mixed cone and rod responses. The b-wave amplitude of the rod response and the a-wave amplitude of the mixed cone and rod response were analyzed.

SD-OCT

After ERG recording, rabbits were placed on a platform such that the visual streaks, which were approximately 3 mm ventral to the ONH, were located at the center of the image. The SD-OCT machine used in this study was *Multiline* OCT (Heidelberg Engineering, Heidelberg, Germany), which was customized based on a Spectralis HRA+OCT [37]. The *Multiline* OCT uses an 870-nm super-luminescent diode as a light source. The scan rate of the SD-OCT was 47,000 A-scans per second, with an axial resolution of ~7 μm.

Measurement and evaluations of total retinal thickness by using SD-OCT

To measure the total retinal thickness at the visual streak, a volume scan image was obtained (Fig. S2A). The lines of the vitreoretinal interface and BM were manually delineated at each horizontal section in a masked fashion (Figs. S2B and S2C). The mean total retinal thickness was measured within a red circle 1 mm in diameter, the center of which was 3 mm ventral to the inferior edge of the ONH, as determined by the software supplied by Heidelberg Engineering (Figs. S2D and S2E).

Measurements and evaluation of the thickness of retinal layers on vertical SD-OCT images

To measure and assess the thickness of each retinal layer, vertical OCT images, which passed through the center of the ONH and included the visual streak, were obtained by averaging 100 B-scans. To measure the thickness of the ONL, ELM–BM, INL, and GCC, the boundary lines between the OPL and ONL, ELM and BM, IPL and INL, and the vitreoretinal interface and IPL were manually delineated in a masked fashion (Fig. S3). The thickness of each retinal layer within the areas (0.5 mm each) 4 mm ventral to the lower edge of the ONH was measured as a function of distance from the lower optic disc margin by using the software supplied by Heidelberg Engineering (Fig. S3).

Electron Microscopy

The enucleated rabbit eyes were fixed in the same manner as the H&E stain. The eyes were subsequently fixed in 1% osmium tetroxide for 90 min. The retina was dehydrated through a graded series of ethanol (50–100%), cleared in propylene oxide, and embedded in epoxy resin. Ultrathin sections were cut by using an ultramicrotome and stained with uranyl acetate and lead citrate. For ultrastructural immunohistochemistry, the enucleated RP rabbit eyes were fixed in 4% paraformaldehyde and 0.05% glutaraldehyde for 4 h. The fixed retina was cut with a microslicer (Microslicer DTK-1000, Dosaka EM, Kyoto, Japan) into sections with a thickness of 65 μm. The sections were incubated with mouse monoclonal anti-rhodopsin antibody (Ret-P1 (sc-57433), Santa Cruz, California, U.S.A.) and subsequently, with gold-conjugated Fab fragment of goat anti-mouse IgG (Nanogold, Molecular Probes, Inc., Oregon, U.S.A.), followed by silver enhancement (HQ Silver, Nanoprobes, Inc., New York, U.S.A.). The stained sections were observed by transmission electron microscopy (H-7650, Hitachi Co., Tokyo, Japan).

Statistical analysis

Data from WT and RP rabbits were analyzed with an unpaired *t*-test by using PASW Statistics version 18.0 (SPSS Inc., Chicago, IL). The level of statistical significance was set at $P<0.05$.

Supporting Information

Figure S1 Ultrastructure of photoreceptors in 20-week-old WT and RP rabbits. (A, B) Ultrastructure of photoreceptors in 20-week-old WT rabbits. The inner segments of photoreceptors (IS) and the outer segments of photoreceptors (OS) were regular and dense. (C, D) Ultrastructural changes in 20-week-old RP rabbits. The IS and OS were mostly absent, and the residual IS and OS were less organized than those in WT rabbits. In the magnified image (D), many small vesicles (arrowheads) appeared to be cleaved from the IS into the extracellular space around the photoreceptors (arrows).
(TIF)

Figure S2 Measurement of mean total retinal thickness. (A) An infrared image on volume scan mode of SD-OCT. In the volume scan mode, the region ventral to the optic disc, including visual streak (19 lines in vertical 15°× horizontal 30°) was imaged. (B) One of the 19 horizontal OCT sections on volume scan mode. The lines of the vitreoretinal interface and the Bruch's membrane are manually delineated at each horizontal section (C). (D) The retinal thickness map constructed from the volume scan OCT images. Total retinal thickness was measured within the red circle shown (E). The diameter of the red circle was 1 mm, and the center was 3 mm ventral to the inferior edge of the ONH (D, E).
(TIF)

Figure S3 Measurement of the thickness of individual retinal layers. Four vertical OCT sections that pass through the center of the ONH and visual streak are shown. On each section, the boundary lines between each retinal layer were manually delineated. The ONL, ELM–BM, INL, and GCC thicknesses were evaluated in 0.5-mm segments as a function of the distance from the inferior optic disc margin up to 4.0 mm ventral to the inferior edge of the ONH. ONL, outer nuclear layer; ELM, external limiting membrane; BM, Bruch's membrane; INL, inner nuclear layer; and GCC, ganglion cell complex.
(TIF)

Acknowledgments

We thank MichikoTsuji, Yuri Terado, and Noriko Suzuki for their technical assistance; Megan Oliver for critical reading of the manuscript; Yuji Nishizawa of Chubu University for his advice on immunohistochemistry; and Gerhald Zinser of Heidelberg Engineering for discussion on the *Multiline* OCT. Presented in part at the Association Research in Vision and Ophthalmology (ARVO) Annual Meeting, May 2011; Florida, U.S.A.

Author Contributions

Conceived and designed the experiments: HOI YM NY. Performed the experiments: YM NN MH MK HT AK. Analyzed the data: YM. Contributed reagents/materials/analysis tools: YT KOF HK. Wrote the paper: YM HOI.

References

1. Hartong DT, Berson EL, Dryja TP (2006) Retinitis pigmentosa. Lancet 368: 1795–1809.
2. Mendes HF, van der Spuy J, Chapple JP, Cheetham ME (2005) Mechanisms of cell death in rhodopsin retinitis pigmentosa: implications for therapy. Trends Mol Med 11: 177–185.
3. Petters RM, Alexander CA, Wells KD, Collins EB, Sommer JR, et al. (1997) Genetically engineered large animal model for studying cone photoreceptor survival and degeneration in retinitis pigmentosa. Nat Biotechnol 15: 965–970.
4. Narfström K (1983) Hereditary progressive retinal atrophy in the Abyssinian cat. J Hered 74: 273–276.
5. Chader GJ (2002) Animal models in research on retinal degenerations: past progress and future hope. Vision Res 42: 393–399.
6. Petersen-Jones SM (1998) Animal models of human retinal dystrophies. Eye (Lond) 12(Pt 3b): 566–570.
7. Barnett KC, Curtis R (1985) Autosomal dominant progressive retinal atrophy in Abyssinian cats. J Hered 76: 168–170.
8. Menotti-Raymond M, David VA, Schäffer AA, Stephens R, Wells D, et al. (2007) Mutation in CEP290 discovered for cat model of human retinal degeneration. J Hered 98: 211–220.
9. Kijas JW, Cideciyan AV, Aleman TS, Pianta MJ, Pearce-Kelling SE, et al. (2002) Naturally occurring rhodopsin mutation in the dog causes retinal dysfunction and degeneration mimicking human dominant retinitis pigmentosa. Proc Natl Acad Sci U S A 99: 6328–6333.
10. Ng YF, Chan HH, Chu PH, To CH, Gilger BC, et al. (2008) Multifocal electroretinogram in rhodopsin P347L transgenic pigs. Invest Ophthalmol Vis Sci 49: 2208–2215.
11. Famiglietti EV, Sharpe SJ (1995) Regional topography of rod and immunocytochemically characterized "blue" and "green" cone photoreceptors in rabbit retina. Vis Neurosci 12: 1151–1175.
12. Rockhill RL, Daly FJ, MacNeil MA, Brown SP, Masland RH (2002) The diversity of ganglion cells in a mammalian retina. J Neurosci 22: 3831–3843.
13. Marc RE (1986) Neurochemical stratification in the inner plexiform layer of the vertebrate retina. Vision Res 26: 223–238.
14. Vaney DI, Young HM, Gynther IC (1991) The rod circuit in the rabbit retina. Vis Neurosci 7: 141–154.
15. Osakada F, Hirami Y, Takahashi M (2009) Stem cell biology and cell transplantation therapy in the retina. Biotechnol Genet Eng Rev 26: 297–334.
16. Stanzel BV, Liu Z, Brinken R, Braun N, Holz FG, et al. (2012) Subretinal delivery of ultrathin rigid-elastic cell carriers using a metallic shooter instrument and biodegradable hydrogel encapsulation. Invest Ophthalmol Vis Sci 53: 490–500.
17. Acland GM, Aguirre GD, Ray J, Zhang Q, Aleman TS, et al. (2001) Gene therapy restores vision in a canine model of childhood blindness. Nat Genet 28: 92–95.
18. Tao W, Wen R, Goddard MB, Sherman SD, O'Rourke PJ, et al. (2002) Encapsulated cell-based delivery of CNTF reduces photoreceptor degeneration in animal models of retinitis pigmentosa. Invest Ophthalmol Vis Sci 43: 3292–3298.
19. Bush RA, Lei B, Tao W, Raz D, Chan CC, et al. (2004) Encapsulated cell-based intraocular delivery of ciliary neurotrophic factor in normal rabbit: dose-dependent effects on ERG and retinal histology. Invest Ophthalmol Vis Sci 45: 2420–2430.
20. Kondo M, Sakai T, Komeima K, Kurimoto Y, Ueno S, et al. (2009) Generation of a transgenic rabbit model of retinal degeneration. Invest Ophthalmol Vis Sci 50: 1371–1377.
21. Wojtkowski M, Bajraszewski T, Gorczynska I, Targowski P, Kowalczyk A, et al. (2004) Ophthalmic imaging by spectral optical coherence tomography. Am J Ophthalmol 138: 412–419.
22. Chen TC, Cense B, Pierce MC, Nassif N, Park BH, et al. (2005) Spectral domain optical coherence tomography: ultra-high speed, ultra-high resolution ophthalmic imaging. Arch Ophthalmol 123: 1715–1720.
23. Sakamoto A, Hangai M, Yoshimura N (2008) Spectral-domain optical coherence tomography with multiple B-scan averaging for enhanced imaging of retinal diseases. Ophthalmology 115: 1071–1078.

24. Hangai M, Yamamoto M, Sakamoto A, Yoshimura N (2009) Ultrahigh-resolution versus speckle noise-reduction in spectral-domain optical coherence tomography. Opt Express 17: 4221–4235.
25. Byeon SH, Chu YK, Lee H, Lee SY, Kwon OW (2009) Foveal ganglion cell layer damage in ischemic diabetic maculopathy: correlation of optical coherence tomographic and anatomic changes. Ophthalmology 116: 1949–1959.
26. Nakano N, Hangai M, Nakanishi H, Mori S, Nukada M, et al. (2011) Macular Ganglion Cell Layer Imaging in Preperimetric Glaucoma with Speckle Noise-Reduced Spectral Domain Optical Coherence Tomography. Ophthalmology 118: 2414–2426.
27. Sandberg MA, Brockhurst RJ, Gaudio AR, Berson EL (2005) The association between visual acuity and central retinal thickness in retinitis pigmentosa. Invest Ophthalmol Vis Sci 46: 3349–3354.
28. Costa RA, Calucci D, Skaf M, Cardillo JA, Castro JC, et al. (2004) Optical coherence tomography 3: Automatic delineation of the outer neural retinal boundary and its influence on retinal thickness measurements. Invest Ophthalmol Vis Sci 45: 2399–2406.
29. Chen TC, Cense B, Miller JW, Rubin PA, Deschler DG, et al. (2006) Histologic correlation of in vivo optical coherence tomography images of the human retina. Am J Ophthalmol 141: 1165–1168.
30. Oishi A, Hata M, Shimozono M, Mandai M, Nishida A, et al. (2010) The significance of external limiting membrane status for visual acuity in age-related macular degeneration. Am J Ophthalmol 150: 27–32.
31. Murakami T, Nishijima K, Sakamoto A, Ota M, Horii T, et al. (2011) Association of pathomorphology, photoreceptor status, and retinal thickness with visual acuity in diabetic retinopathy. Am J Ophthalmol 151: 310–317.
32. Huber G, Beck SC, Grimm C, Sahaboglu-Tekgoz A, Paquet-Durand F, et al. (2009) Spectral domain optical coherence tomography in mouse models of retinal degeneration. Invest Ophthalmol Vis Sci 50: 5888–5895.
33. Kim KH, Puoris'haag M, Maguluri GN, Umino Y, Cusato K, et al. (2008) Monitoring mouse retinal degeneration with high-resolution spectral-domain optical coherence tomography. J Vis 8: 17 1–11.
34. Ruggeri M, Wehbe H, Jiao S, Gregori G, Jockovich ME, et al. (2007) In vivo three-dimensional high-resolution imaging of rodent retina with spectral-domain optical coherence tomography. Invest Ophthalmol Vis Sci 48: 1808–1814.
35. Srinivasan VJ, Ko TH, Wojtkowski M, Carvalho M, Clermont A, et al. (2006) Noninvasive volumetric imaging and morphometry of the rodent retina with high-speed, ultrahigh-resolution optical coherence tomography. Invest Ophthalmol Vis Sci 47: 5522–5528.
36. Fischer MD, Huber G, Beck SC, Tanimoto N, Muehlfriedel R, et al. (2009) Noninvasive, in vivo assessment of mouse retinal structure using optical coherence tomography. PLoS ONE 4: 1–7.
37. Nakano N, Ikeda HO, Hangai M, Muraoka Y, Toda Y, et al. (2011) Longitudinal and Simultaneous Imaging of Retinal Ganglion Cells and Inner Retinal Layers in a Mouse Model of Glaucoma Induced by N-Methyl-D-Aspartate. Invest Ophthalmol Vis Sci 52: 8754–8762.
38. Yamauchi Y, Agawa T, Tsukahara R, Kimura K, Yamakawa N, et al. (2011) Correlation between high-resolution optical coherence tomography (OCT) images and histopathology in an iodoacetic acid-induced model of retinal degeneration in rabbits. Br J Ophthalmol 95: 1161–1165.
39. Li T, Snyder WK, Olsson JE, Dryja TP (1996) Transgenic mice carrying the dominant rhodopsin mutation P347S: evidence for defective vectorial transport of rhodopsin to the outer segments. Proc Nad Acad Sci U S A 93: 14176–14181.
40. Aleman TS, Cideciyan AV, Sumaroka A, Windsor EA, Herrera W, et al. (2008) Retinal laminar architecture in human retinitis pigmentosa caused by Rhodopsin gene mutations. Invest Ophthalmol Vis Sci 49: 1580–1590.
41. Milam AH, Li ZY, Fariss RN (1998) Histopathology of the human retina in retinitis pigmentosa. Prog Retin Eye Res 17: 175–205.
42. Humayun MS, Prince M, de Juan E, Jr., Barron Y, Moskowitz M, et al. (1999) Morphometric analysis of the extramacular retina from postmortem eyes with retinitis pigmentosa. Invest Ophthalmol Vis Sci 40: 143–148.

Transcorneal Electrical Stimulation Promotes Survival of Photoreceptors and Improves Retinal Function in Rhodopsin P347L Transgenic Rabbits

Takeshi Morimoto,[1] *Hiroyuki Kanda,*[1] *Mineo Kondo,*[2] *Hiroko Terasaki,*[3] *Kohji Nishida,*[4] *and Takashi Fujikado*[1]

Purpose. To determine whether transcorneal electrical stimulation (TES) has neuroprotective effects on the photoreceptors, and whether it slows the rate of decrease of the electroretinogram (ERG) in rhodopsin P347L transgenic (Tg) rabbits.

Methods. Six-week-old Tg rabbits received TES through a contact lens electrode on the left eye weekly for 6 weeks. The right eyes received sham stimulation on the same days. Electroretinograms (ERGs) were recorded before and at 12 weeks after the TES. After the last ERG recordings, the animals were euthanized for morphologic analysis of the retinas. Immunohistochemical (IHC) analysis was performed to detect the immunostaining by peanut agglutinin (PNA) and rhodopsin antibodies in the retinas.

Results. The a- and b-wave amplitudes of the photopic ERGs and the b-wave amplitudes of the scotopic ERGs at higher stimulus intensities were significantly larger in the TES eyes than in the sham stimulated eyes ($P < 0.05$, respectively). Morphologic analyses showed that the mean thickness of the outer nuclear layer (ONL) in the visual streak at 12 weeks was significantly thicker in TES eyes than in sham-stimulated eyes ($P < 0.05$). IHC showed that the immunostaining by PNA and rhodopsin antibody in the TES-treated retinas was stronger than that in the sham-stimulated retinas.

Conclusions. TES promotes the survival of photoreceptors and preserves the ERGs in Tg rabbits. Although further investigations are necessary before using TES on patients, these findings indicate that TES should be considered for therapeutic treatment for RP patients with a P347L mutation of rhodopsin. (*Invest Ophthalmol Vis Sci.* 2012;53:4254–4261) DOI: 10.1167/iovs.11-9067

Patients with RP have a progressive loss of rod and cone photoreceptors that leads to a severe decrease in the visual acuity and a severe constriction of the visual field.[1,2] The worldwide prevalence of RP is approximately 1 in 4000, meaning that more than 1 million individuals are affected worldwide.[3] As such, RP is one of the leading causes of blindness in the world.

Many promising treatments to save or restore vision in RP patients are being investigated clinically and experimentally.[4–9] Electrical stimulation (ES) of the retina is one of the methods that is being tried because it is less invasive than other treatments and has been shown to have neuroprotective properties on the visual system.[10–18] ES of the transected optic nerve stump in rats promoted the survival of axotomized retinal ganglion cells (RGCs) in vivo.[10] Transcorneal electrical stimulation (TES) in rats was reported to rescue axotomized RGCs[11,12] and promote axonal regeneration of injured RGCs.[13,14] TES was also shown to improve the visual function of patients with traumatic optic neuropathy and nonarteritic ischemic optic neuropathy.[15]

We have demonstrated that TES promoted the survival of photoreceptors and preserved the retinal function of Royal College of Surgeons (RCS) rats, an animal model of RP.[16] Ni et al.[17] also reported that TES had neuroprotective effects on the photoreceptors after phototoxicity in rats. In a preliminary clinical trial, Schatz et al.[18] demonstrated that TES improved the visual function in RP patients.

However, RP is a genetically heterogeneous disease, and mutations in several photoreceptor-specific and some non-specific genes are known to cause RP.[19] Therefore, it is necessary to examine the neuroprotective effect of TES on the photoreceptors in the retinas of various RP animal models to determine which genetic type of RP is responsive to TES.

Rhodopsin Pro 347 Leu (P347L) transgenic (Tg) rabbits have been generated by Kondo et al.[20] This sequence of alterations is similar to those in human patients with autosomal dominant RP (adRP) with the rhodopsin P347L mutation.[21,22] This animal model has a rod-dominated, progressive photoreceptor degeneration with regional variations in the pattern of photoreceptor loss.[20,23]

The purpose of this study was to determine whether TES has a neuroprotective effect on the photoreceptors and improves the amplitudes of the electroretinogram (ERG) in Tg rabbits. Our morphologic and electrophysiological analyses showed that TES had a neuroprotective effect on the photoreceptors and improved the amplitudes of the ERG of Tg rabbits.

Materials and Methods

Animals

All experimental procedures were performed in accordance with the ARVO Statement for the Use of Animals in Ophthalmic and Vision

From the [1]Departments of Applied Visual Science and [4]Ophthalmology, Osaka University Graduate School of Medicine, Osaka, Japan; [2]Department of Ophthalmology, Mie University Graduate School of Medicine, Mie, Japan; and [3]Department of Ophthalmology, Nagoya University Graduate School of Medicine, Nagoya, Japan.

Submitted for publication November 12, 2011; revised April 3, 2012; accepted April 25, 2012.

Disclosure: **T. Morimoto**, None; **H. Kanda**, None; **M. Kondo**, None; **H. Terasaki**, None; **K. Nishida**, None; **T. Fujikado**, None

Corresponding author: Takeshi Morimoto, Department of Applied Visual Science, Osaka University Graduate School of Medicine, 2-2 Yamadaoka, Suita City, Osaka 565-0871, Japan; takeshi.morimoto@ophthal.med.osaka-u.ac.jp.

Investigative Ophthalmology & Visual Science, June 2012, Vol. 53, No. 7

Research, and the procedures were approved by the Animal Research Committee, Osaka University Graduate School of Medicine. Five Tg rabbits were purchased from the Kitayama Labes Co. (Ina, Japan). They were raised on a 12-hour dark 12-hour light cycle with an ambient light intensity of 100 lux.

Transcorneal Electrical Stimulation

The rabbits were anesthetized intramuscularly with a mixture of medetomidine (0.3 mg/kg, Domitor; Orion Corporation, Espoo, Finland), midazolam (4 mg/kg, Dormicum, Astellas Pharma Inc., Tokyo, Japan), and butorphanol (5 mg/kg, Betorphal; Meiji Seika Pharma, Co., Ltd., Tokyo, Japan). For the electrical stimulation, the corneas were also anesthetized with a drop of 0.4% oxybuprocaine HCl, and a contact lens electrode with inner and outer concentric electrodes (Mayo Corporation, Nagoya, Japan) was placed on the cornea with a drop of 2.5% methylcellulose to maintain good electrical contact and prevent corneal drying. Biphasic rectangular current pulses (700 μA, 10 ms/phase duration) were delivered at a frequency of 20 Hz from an electrical stimulation system (Stimulator: SEN-7320, Nihon Kohden, Tokyo, Japan; Isolator: WPI, Sarasota, FL) through the contact lens electrode.

TES was given to 6-week-old rabbits for 1 hour once a week until the animals were 12 weeks old. Only the left eye was electrically stimulated. The same type of contact lens electrode was placed on the right eyes but no electrical current was delivered (sham stimulation).

Electroretinograms

ERGs were recorded from the animals at 6 weeks of age just before the beginning of the TES and after the end of the TES treatments at 12 weeks of age. For the TES, animals were anesthetized intramuscularly with a mixture of medetomidine (0.3 mg/kg), midazolam (1 mg/kg), and butorphanol (1 mg/kg). The pupils were dilated with 2.5% phenylephrine hydrochloride and 0.5 % tropicamide.

After 1 hour of dark adaptation, the animals were restrained in a box and were prepared for the recordings under dim red light. ERGs were recorded from both eyes simultaneously with a corneal electrode carrying LEDs creating a mini-Ganzfeld stimulator (WLS-20, Mayo Corporation). A 2.5% hydroxypropyl methylcellulose ophthalmic solution was used with the corneal contact lens electrode. The reference electrode and a ground electrode were inserted subcutaneously into the left ear and the nose, respectively.

The luminance of the scotopic ERG stimuli was increased from −5.0 to 1.48 log cd·s/m^2 in 0.5 or 1.0 log unit steps. After the scotopic ERG recordings, animals were light-adapted for 30 minutes, and the photopic ERGs were recorded. The luminance of photopic ERG stimuli was increased from −1.0 to 1.95 log cd·s/m^2, and the stimuli were presented on a white background of 25 cd/m^2.

The responses were amplified, band pass filtered from 0.3 to 1000 Hz, and digitized at 3.3 kHz. A computational ERG recording system (Neuropack μ; Nihon Kohden, Tokyo, Japan) was used to average the ERG responses. Five to 20 responses were averaged with interstimulus intervals from 1 to 10 seconds depending on the intensity of the stimulus.

ERG Analysis

The scotopic (dark-adapted) and photopic (light-adapted) a-wave amplitudes were measured from the prestimulus baseline to the peak of the a-wave, and the b-wave amplitude was measured from the trough of the a-wave to the peak of b-wave.

To determine the significance of differences in the ERG amplitudes between TES electrically stimulated eyes and sham-stimulated eyes for the full intensity range, we plotted the average ratio of the TES-treated to the sham-stimulated eyes at all intensities and performed statistical analyses.[22–24]

Histological Analysis

Immediately after the final ERG recordings, the rabbits were euthanized with an overdose of pentobarbital sodium. The eyes were removed and placed in a mixture of 10% neutral buffered formalin and 2.5% glutaraldehyde in 0.1 M phosphate buffer (PB) for 30 minutes at room temperature. Then eyes were trimmed, and part of the eye cups, including the optic nerve, were postfixed in 4% glutaraldehyde in 0.1 M PB at 4°C. The tissues were trimmed, embedded in paraffin, sectioned vertically, and stained with hematoxylin and eosin for light microscopy. All sections were cut along the vertical meridian of the eye passing through the optic nerve. Five serial sections of each eye were analyzed for each experimental animal.

The degree of retinal degeneration was assessed by measuring the thickness of the outer nuclear layer (ONL), inner nuclear layer (INL), and ganglion cell layer (GCL). Photographs were taken of the superior and inferior hemispheres at 10 defined points with a camera attached to a light microscope (E800; Nikon, Tokyo, Japan). The first photograph was taken at approximately 2 mm from the center of the optic nerve head, and subsequent photographs were taken every 2 mm more peripherally. The thickness of ONL, INL, and GCL were measured on the photographs (Scion Image analyzer; Scion Corp., Frederick, MD). Each eye was coded so that the investigator making the measurements was masked to treatment of the eye.

Immunohistochemistry

The paraffin-embedded sections (5 μm) were processed for immunofluorescence staining with antirhodopsin antibody (1:100; RET-P1; Santa Cruz Biotechnology, Santa Cruz, CA), followed by Cy3-conjugated anti-mouse IgG (1:200), and FITC-conjugated peanut agglutinin (1:100) (PNA; Invitrogen, Carlsbad, CA), a lectin that binds specifically to rabbit cone photoreceptors. The TES-treated and sham-stimulated sections were observed with a fluorescence microscope (E800; Nikon).

Statistical Analysis

Data were analyzed with a commercial software (JMP8; SAS Institute Japan, Tokyo, Japan). The data were expressed as the means ± SDs or SEMs. Comparisons between two groups were made by Student's *t*-tests when the data were normally distributed or by the Mann-Whitney rank-sum test when the data were not normally distributed. Statistical significance was set at $P < 0.05$.

Results

Effect of TES on Survival of Photoreceptors in Tg Rabbits

Representative retinal sections in the area of the visual streak from 12-week-old Tg rabbits that had TES (left eye) or sham stimulation (right eye) are shown in Figures 1A and 1B. The number of rows of nuclei in the ONL at the visual streak was two to three and the nuclei were closely packed in the retina receiving TES (Fig. 1A). In the sham-stimulated retina, only one row of nuclei was found in the ONL at the visual streak and they were loosely packed (Fig. 1B). In contrast, there was no difference in the structure and thickness of the ONL in other areas of the retina away from the visual streak between the TES-treated and sham-stimulated retinas (Figs. 1C, 1D). The architecture and thickness of the middle and inner retinal layers were well preserved in both TES-treated and sham-stimulated retinas (Figs. 1A–D).

Quantitative analyses showed that the thickness of the ONL in the visual streak in the TES-treated eyes was 13.9 ± 3.3 μm

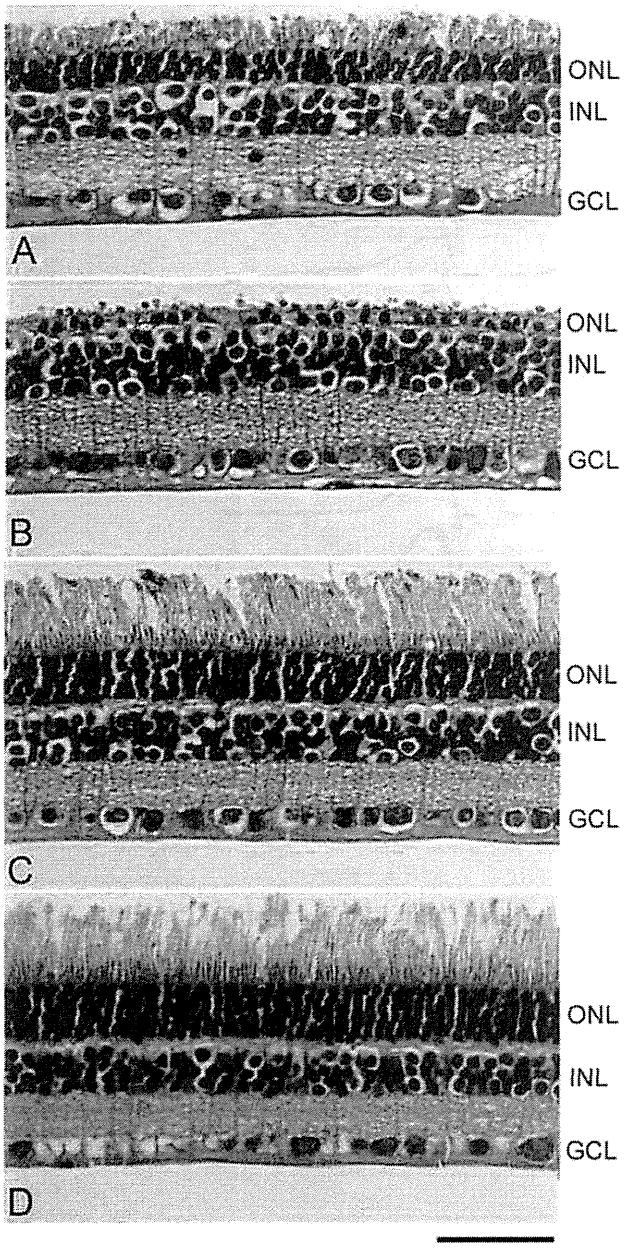

FIGURE 1. Photomicrographs of TES-treated and sham-stimulated retinas from 12-week-old Tg rabbits. Retinal sections of the visual streak from TES-treated retina (A) and sham-stimulated retina (B). Peripheral retinas at 6 mm superior to the optic nerve head from TES-treated retina (C) and sham-stimulated retina (D). Scale bar = 50 μm.

(mean ± SD, $n = 5$) which was significantly thicker than that in the sham-stimulated eyes (8.8 ± 2.8 μm, $n = 5$, $P < 0.05$) (inferior hemisphere 1). In contrast, there was no significant difference in the mean ONL thickness outside the area of the visual streak (Fig. 2A). Thus, TES promoted the survival of photoreceptors in the area of the visual streak at 12 weeks of age.

To determine whether TES affected other layers of the retina, we measured the thickness of the INL and GCL. There were no significant differences of the mean thickness of INL and GCL between the TES retinas and in the sham retinas ($n = 5$ each; Figs. 2B, 2C).

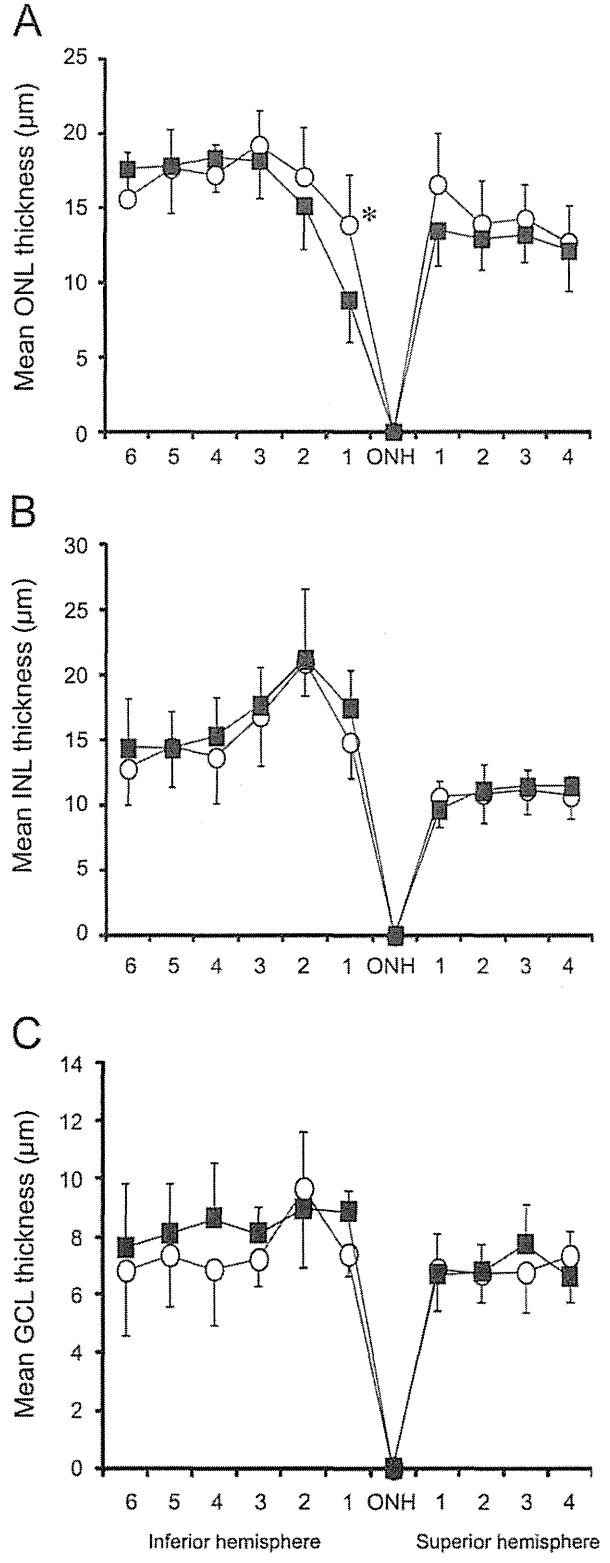

FIGURE 2. Thickness of the ONL (A), the INL (B), and the GCL (C) along the vertical meridian measured at 10 retinal locations at 2-mm intervals. Mean ± SD of five Tg rabbits are plotted. There was a significant difference of the mean ONL thickness between TES-treated retinas (○) and sham-stimulated retina (■) at the visual streak (Student's *t*-test for two groups; $^*P < 0.05$).

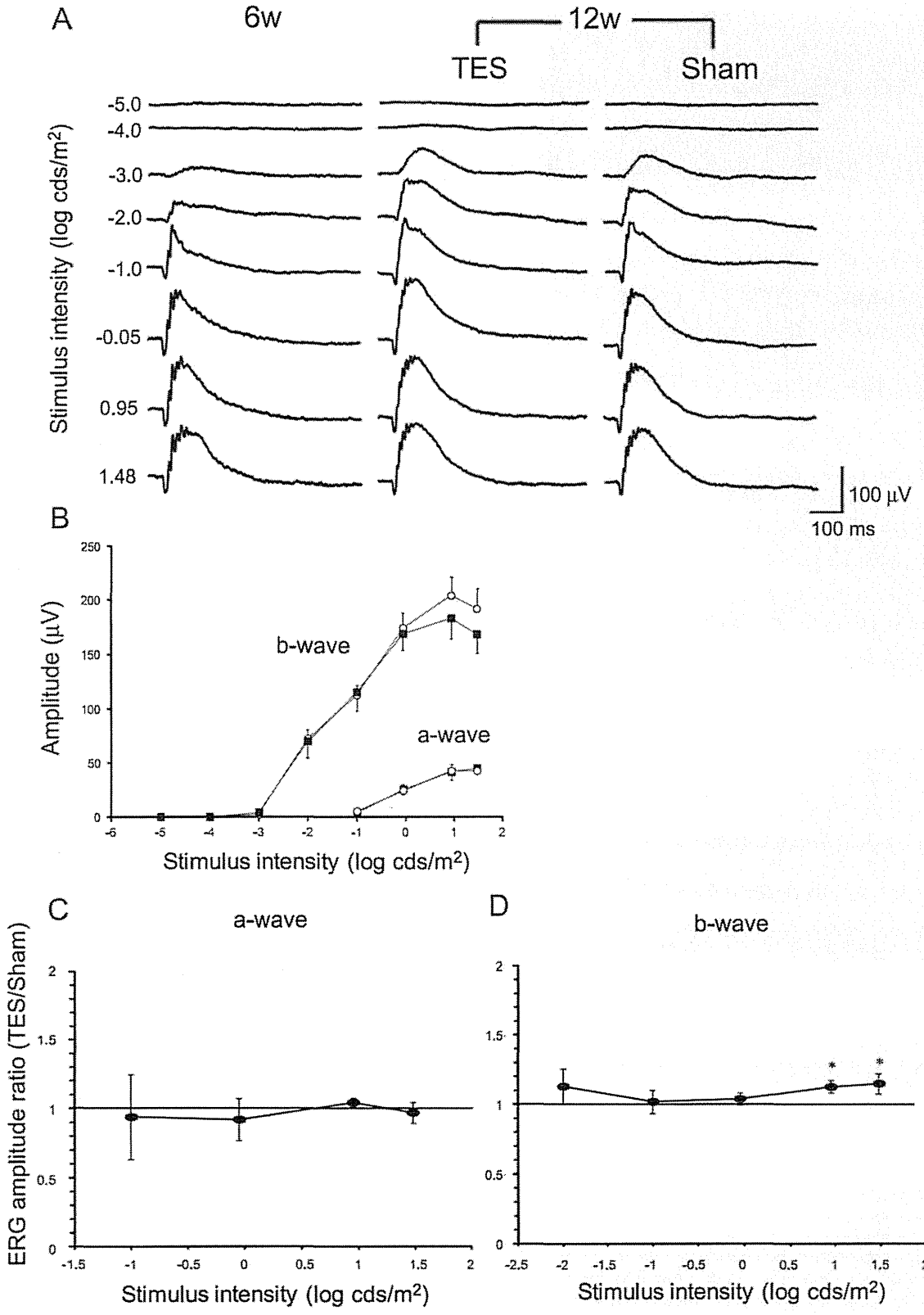

FIGURE 3. Scotopic ERGs recorded from 6- and 12-week-old rhodopsin P347L Tg rabbits. (A) Scotopic ERGs elicited by eight different stimulus intensities. (B) Scotopic ERG mean amplitude versus flash intensity for the a- and b-waves in the TES-treated (○) and sham-stimulated eyes (■) ($n = 5$, each, mean ± SEM). Average ratio (TES/sham) of the a- (C) and b-wave (D) amplitudes at 12 weeks of age ($n = 5$, each, mean ± SEM). Pointwise comparison indicated a significant difference in b-wave amplitudes at 1.48 and 0.95 log cd-s/m² (Student's *t*-tests for two groups; $^*P < 0.05$).

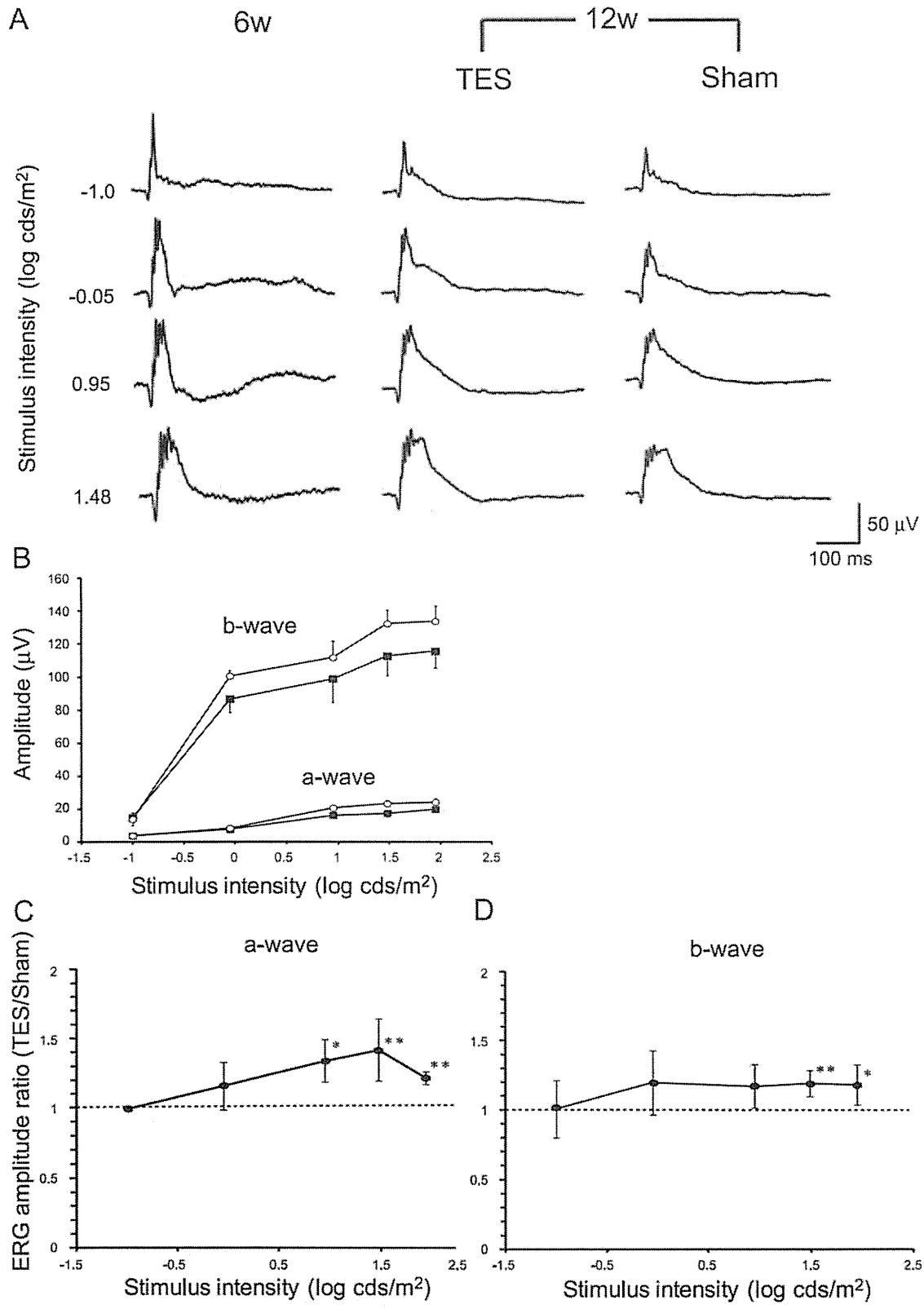

FIGURE 4. Photopic ERGs recorded from 6- and 12-week-old rhodopsin P347L Tg rabbits. (A) Photopic ERGs elicited by five different stimulus intensities. (B) Photopic ERG mean amplitude versus flash intensity for the a- and b-waves in the TES-treated (○) and sham-stimulated (■) retinas. Average ratio (TES/sham) of the a- (C) and b-wave (D) amplitudes at 12 weeks of age ($n = 5$, each, mean ± SEM). Pointwise comparison indicated a significant difference in a-wave amplitudes at 0.95 to 1.95 log cd-s/m² (Student's t-tests for two groups; $^{*}P < 0.05$, $^{**}P < 0.01$), and in b-wave amplitudes at 1.48 and 1.95 log cd-s/m² (Student's t-tests for two groups; $^{*}P < 0.05$, $^{**}P < 0.01$).

Effect of TES on Electroretinograms of Tg Rabbits

To evaluate the electrical properties of the rod and cone systems of rabbits, we recorded full-field scotopic and photopic ERGs. The scotopic ERGs elicited by different stimulus intensities from 6- and 12-week-old Tg rabbits are shown in Figure 3A. The amplitudes of the scotopic ERGs recorded from the eyes of 12-week-old Tg rabbits were not reduced compared with those from the eyes of 6-week-old Tg rabbits. The intensity–response curves for the a- and b-waves are plotted in Figure 3B. Scotopic ERG a-wave amplitudes of TES-treated eyes were not significantly different from those of sham-stimulated eyes. However, the b-wave amplitudes of the TES-treated eyes were slightly but significantly larger than those of the sham-stimulated eyes at the higher stimulus intensities.

We plotted the ratio (TES/sham-stimulated eye) of the amplitudes of the a- and b-waves for all intensities and performed statistical analyses on the differences (Figs. 3C, 3D). The differences in the ratios of the a-waves were not significant for all intensities. On the other hand, the ratios of the b-wave amplitudes were significantly larger at stimulus intensities higher than 0.95 log cd·s/m^2 ($P < 0.05$) in the TES-treated eyes.

The photopic ERGs obtained from Tg rabbits at 6 and 12 weeks of age are also shown in Figure 4A. The amplitudes of the TES-treated and sham-stimulated eyes at 12 weeks of age were slightly reduced compared with the ERGs recorded from 6-week-old Tg rabbits but the differences were not significant. However, the responses in the eye treated with TES were larger than those treated with sham stimulation (Fig. 4A).

The intensity–response curve for the a- and b-waves are plotted in Figure 4B. We also plotted the average ratio of TES-treated to sham-stimulated eyes at all intensities (Figs. 4C, 4D). For a-waves, there were significant differences between TES-treated and sham-stimulated eyes at 0.95 to 1.95 log cd·s/m^2 ($P < 0.05$, respectively). For b-waves, there were significant differences between them at 1.48 and 1.95 log cds/m^2 ($P < 0.05$).

Immunohistochemistry

Immunostaining with an antirhodopsin antibody and PNA lectin showed that the intensities of the immunostaining for both antirhodopsin antibody and PNA were stronger in the TES-treated retina (Figs. 5A–C) than the sham-stimulated retina (Figs. 5D–F).

Discussion

Our electrophysiological and histological analyses showed that TES led to the survival of photoreceptors in the visual streak, and it also led to the preservation of ERG responses at higher stimulus intensities in rhodopsin P347L Tg rabbits. Although the cause of the photoreceptor degeneration in Tg rabbits is different from that in RCS rats and the phototoxic-induced degeneration in rats,[20,23,25–27] TES also had a neuroprotective effect on the photoreceptors in Tg rabbits. These findings indicate that TES might have a similar neuroprotective effect on photoreceptors whose degeneration has different causes.

In the histological analysis, only the photoreceptors in the visual streak were rescued by TES, and in the areas outside the visual streak, the number of photoreceptors in the TES-treated retina was not significantly different from that in sham-stimulated retina. In Tg rabbits, the loss of photoreceptors was maximum in the visual streak where the photoreceptor density is highest, and the loss of photoreceptors was not significantly different at other regions outside visual streak at 12 weeks of age.[20] Therefore, at 12 weeks of age, the loss of photoreceptors was striking only in the visual streak, indicating that the neuroprotection of photoreceptors was limited to the visual streak.

Immunohistochemical analysis showed that the intensity of both PNA and rhodopsin immunostainings was stronger in the TES-treated retinas than in the sham-stimulated retinas in the visual streak.

However, the results of ERGs indicated that TES preserved the cone components better than rod components, although in Tg rabbits the rod components are more affected than the cones.[20,23] Although it was not determined why the cone components were better preserved than the rod components, one possibility is that TES promoted the survival of both rod and cone photoreceptors, and the rescued rods secreted a cone viability factor to rescue the cone photoreceptors.[28] Otherwise, at 12 weeks of age, photoreceptors near the visual streak were much more affected than those outside the visual streak,[20] therefore the differences of ERG amplitudes of full field ERGs between TES-treated and sham-stimulated retinas might be detected only at higher stimulus intensities.

There are some possible mechanisms for the neuroprotection of photoreceptors. First, TES increased the expression of the mRNA and protein levels of neurotrophic factors (e.g., insulin-like growth factor-1 (IGF-1), brain-derived neurotrophic

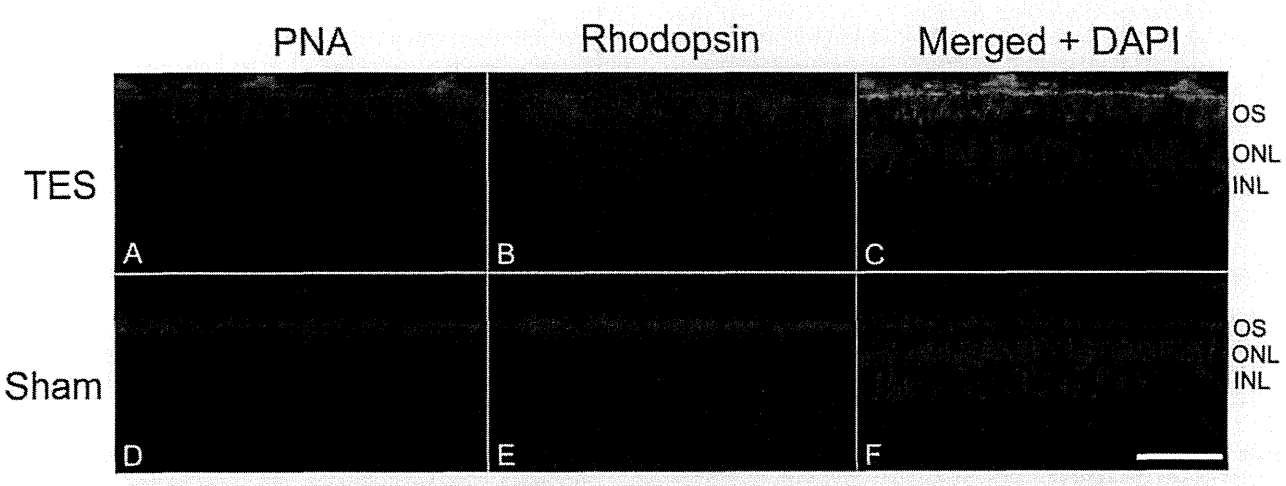

Figure 5. Immunohistochemical analysis of rod and cone photoreceptors triple labeled with rhodopsin (*green*), PNA (*red*), and DAPI (*blue*) in TES-treated (**A–C**) and sham-stimulated retinas (**D–E**) at 12 weeks of age (approximately 4 mm inferior to the optic nerve head). Intensities of rhodopsin and PNA immunostaining are stronger in the TES-treated ratio than in the sham-stimulated retina. Scale bar = 50 μm.

factor (BDNF), ciliary neurotrophic factor, or B-cell lymphoma-2 in the retinas after TES.[11,17] A second possibility is that TES reduced the expression of the TNF super families and Bax, which are related to apoptosis signaling in retinal cells.[29] Cultured rat Müller cells exposed to electrical currents have been shown to express IGF-1, BDNF, and fibroblast growth factor-2 (FGF-2).[30–32] Other types of electrical stimulation to the retinas, such as subretinal electrical stimulation, increases the expression of FGF-2 in the retinas.[33] Unfortunately, we did not determine whether the expression of any of these neurotrophic factors was increased after TES in the Tg rabbit retinas.

Another possible mechanism for the TES-induced neuroprotection was an increase of chorioretinal blood circulation by TES.[34,35] In clinical studies, TES has been shown to improve the visual function of patients with retinal artery occlusion.[36,37] Thinning of the vascular plexus and the development of aberrant vessels have been reported in RP patients and animal models of RP.[38–41] This indicates that retinal blood circulation might be reduced in Tg rabbits. TES might have some neuroprotective effects on photoreceptors by increasing chorioretinal blood circulation.

We did not examine whether TES was neuroprotective for the photoreceptors in the peripheral retina. In Tg rabbits at the age of 48 weeks, almost all of the photoreceptors were lost[20,27]; however, it takes a long time to investigate the neuroprotective effects of TES on the entire retina until the age of 48 weeks from 6 weeks, so it is difficult to continue the treatment until 48 weeks because weekly anesthesia and treatment put a heavy load on animals and is adverse to the animal welfare for long-term experiments. The results that TES did have neuroprotective effects on photoreceptors in the visual streak at 12 weeks of age were enough to lead us to determine the neuroprotection of TES on the photoreceptors in Tg rabbits.

Rhodopsin P347L Tg rabbits are an adRP model of human RP. Our results indicate that TES might have a neuroprotective effect on the photoreceptors in RP patients with the same mutation. Schatz et al.[18] performed a prospective, randomized sham-controlled clinical study, and reported that TES improved the visual function in RP patients. From these neuroprotective effects of TES already published and our results, TES might exert a neuroprotective effect on photoreceptors of different animals with RP. Additional investigations on different animal models are necessary to determine which type of RP was the indication of TES treatment.

In conclusion, TES had a neuroprotective effect on the photoreceptors in the visual streak of rhodopsin P347L Tg rabbits, which is a model of human adRP. These results support and encourage clinical trials of TES for RP patients.

Acknowledgments

The authors thank Yuko Furukawa and Emi Higasa for technical assistance, and Duco I. Hamasaki for help with the manuscript.

References

1. Marmor MF, Aguirre G, Arden G, et al. Retinitis pigmentosa: a symposium on terminology and methods of examination. *Ophthalmology.* 1983;90:126–131.
2. Pagon RA. Retinitis pigmentosa. *Surv Ophthalmol.* 1988;33:137–177.
3. Hartong DT, Berson EL, Dryja TP. Retinitis pigmentosa. *Lancet.* 2006;368:1795–1809.
4. Berson EL, Rosner B, Sandberg MA, et al. A randomized trial of vitamin A and vitamin E supplementation for retinitis pigmentosa. *Arch Ophthalmol.* 1993;111:761–772.
5. Sieving PA, Caruso RC, Tao W, et al. Ciliary neurotrophic factor (CNTF) for human retinal degeneration: phase I trial of CNTF delivered by encapsulated cell intraocular implants. *Proc Natl Acad Sci U S A.* 2006;103:3896–3901.
6. Ali RR, Sarra GM, Stephens C, et al. Restoration of photoreceptor ultrastructure and function in retinal degeneration slow mice by gene therapy. *Nat Genet.* 2000;25:306–310.
7. Bainbridge JW, Smith AJ, Barker SS, et al. Effect of gene therapy on visual function in Leber's congenital amaurosis. *N Engl J Med.* 2008;358:2231–2239.
8. Zrenner E, Bartz-Schmidt KU, Benav H, et al. Subretinal electronic chips allow blind patients to read letters and combine them to words. *Proc Biol Sci.* 2011;278:1489–1497.
9. Fujikado T, Kamei M, Sakaguchi H, et al. Testing of semichronically implanted retinal prosthesis by suprachoroidal-transretinal stimulation in patients with retinitis pigmentosa. *Invest Ophthalmol Vis Sci.* 2011;52:4726–4733.
10. Morimoto T, Miyoshi T, Fujikado T, Tano Y, Fukuda Y. Electrical stimulation enhances the survival of axotomized retinal ganglion cells in vivo. *NeuroReport.* 2002;13:227–230.
11. Morimoto T, Miyoshi T, Matsuda S, Tano Y, Fujikado T, Fukuda Y. Transcorneal electrical stimulation rescues axotomized retinal ganglion cells by activating endogenous retinal IGF-1 system. *Invest Ophthalmol Vis Sci.* 2005;46:2147–2155.
12. Morimoto T, Miyoshi T, Sawai H, Fujikado T. Optimal parameters of transcorneal electrical stimulation (TES) to be neuroprotective of axotomized RGCs in adult rats. *Exp Eye Res.* 2010;90:285–291.
13. Miyake K, Yoshida M, Inoue Y, Hata Y. Neuroprotective effect of transcorneal electrical stimulation on the acute phase of optic nerve injury. *Invest Ophthalmol Vis Sci.* 2007;48:2356–2361.
14. Tagami Y, Kurimoto T, Miyoshi T, Morimoto T, Sawai H, Mimura O. Axonal regeneration induced by repetitive electrical stimulation of crushed optic nerve in adult rats. *Jpn J Ophthalmol.* 2009;53:257–266.
15. Fujikado T, Morimoto T, Matsushita K, Shimojo H, Okawa Y, Tano Y. Effect of transcorneal electrical stimulation in patients with nonarteritic ischemic optic neuropathy or traumatic optic neuropathy. *Jpn J Ophthalmol.* 2006;50:266–273.
16. Morimoto T, Fujikado T, Choi JS, et al. Transcorneal electrical stimulation promotes the survival of photoreceptors and preserves retinal function in royal college of surgeons rats. *Invest Ophthalmol Vis Sci.* 2007;48:4725–4732.
17. Ni YQ, Gan DK, Xu HD, Xu GZ, Da CD. Neuroprotective effect of transcorneal electrical stimulation on light-induced photoreceptor degeneration. *Exp Neurol.* 2009;219:439–452.
18. Schatz A, Röck T, Naycheva L, et al. Transcorneal electrical stimulation for patients with retinitis pigmentosa: a prospective, randomized, sham-controlled exploratory study. *Invest Ophthalmol Vis Sci.* 2011;23:4485–4496.
19. Daiger SP, Bowne SJ, Sullivan LS. Perspective on genes and mutations causing retinitis pigmentosa. *Arch Ophthalmol.* 2007;125:151–158.
20. Kondo M, Sakai T, Komeima K, et al. Generation of a transgenic rabbit model of retinal degeneration. *Invest Ophthalmol Vis Sci.* 2009;50:1371–1377.
21. Oh KT, Longmuir R, Oh DM, et al. Comparison of the clinical expression of retinitis pigmentosa associated with rhodopsin mutations at codon 347 and codon 23. *Am J Ophthalmol.* 2003;136:306–313.
22. Berson EL, Rosner B, Sandberg MA, et al. Ocular findings in patients with autosomal dominant retinitis pigmentosa and rhodopsin, proline-347-leucine. *Am J Ophthalmol.* 1991;111:614–623.
23. Sakai T, Kondo M, Ueno S, et al. Supernormal ERG oscillatory potentials in transgenic rabbit with rhodopsin P347L mutation

and retinal degeneration. *Invest Ophthalmol Vis Sci.* 2009;50: 4402–4409.

24. Bush RA, Lei B, Tao W, et al. Encapsulated cell-based intraocular delivery of ciliary neurotrophic factor in normal rabbit: dose-dependent effects on ERG and retinal histology. *Invest Ophthalmol Vis Sci.* 2004;45:2420–2430.
25. D'Cruz PM, Yasumura D, Weir J, et al. Mutation of the receptor tyrosine kinase gene Mertk in the retinal dystrophic RCS rat. *Hum Mol Genet.* 2000;9:645–651.
26. Noell WK, Walker VS, Kang BS, Berman S. Retinal damage by light in rats. *Invest Ophthalmol.* 1966;5:450–473.
27. Jones BW, Kondo M, Terasaki H, et al. Retinal remodeling in the Tg P347L rabbit, a large-eye model of retinal degeneration. *J Comp Neurol.* 2011;519:2713–2733.
28. Léveillard T, Mohand-Saïd S, Lorentz O, et al. Identification and characterization of rod-derived cone viability factor. *Nat Genet.* 2004;36:755–759.
29. Willmann G, Schäferhoff K, Fischer MD, et al. Gene expression profiling of the retina after transcorneal electrical stimulation in wildtype brown Norway rats. *Invest Ophthalmol Vis Sci.* 2011;52:7529–7537.
30. Sato T, Lee TS, Takamatsu F, Fujikado T. Induction of fibroblast growth factor-2 by electrical stimulation in cultured retinal Mueller cells. *Neuroreport.* 2008;19:1617–1621.
31. Sato T, Fujikado T, Morimoto T, Matsushita K, Harada T, Tano Y. Effect of electrical stimulation on IGF-1 transcription by L-type calcium channels in cultured retinal Müller cells. *Jpn J Ophthalmol.* 2008;52:217–223.
32. Sato T, Fujikado T, Lee TS, Tano Y. Direct effect of electrical stimulation on induction of brain-derived neurotrophic factor from cultured retinal Müller cells. *Invest Ophthalmol Vis Sci.* 2008;49:4641–4646.
33. Ciavatta VT, Kim M, Wong P, et al. Retinal expression of Fgf2 in RCS rats with subretinal microphotodiode array. *Invest Ophthalmol Vis Sci.* 2009;50:4523–4530.
34. Kurimoto T, Oono S, Oku H, et al. Transcorneal electrical stimulation increases chorioretinal blood flow in normal human subjects. *Clin Ophthalmol.* 2010;4:1441–1446.
35. Mihashi T, Okawa Y, Miyoshi T, Kitaguchi Y, Hirohara Y, Fujikado T. Comparing retinal reflectance changes elicited by transcorneal electrical retinal stimulation with those of optic chiasma stimulation in cats. *Jpn J Ophthalmol.* 2011;55:49–56.
36. Inomata K, Shinoda K, Ohde H, et al. Transcorneal electrical stimulation of retina to treat longstanding retinal artery occlusion. *Graefes Arch Clin Exp Ophthalmol.* 2007;245: 1773–1780.
37. Oono S, Kurimoto T, Kashimoto R, Tagami Y, Okamoto N, Mimura O. Transcorneal electrical stimulation improves visual function in eyes with branch retinal artery occlusion. *Clin Ophthalmol.* 2011;5:397–402.
38. Spalton DJ, Bird AC, Cleary PE. Retinitis pigmentosa and retinal oedema. *Br J Ophthalmol.* 1978;62:174–182.
39. Uliss AE, Gregor ZJ, Bird AC. Retinitis pigmentosa and retinal neovascularization. *Ophthalmology.* 1986;93:1599–1602.
40. Matthes MT, Bok D. Blood vascular abnormalities in the degenerative mouse retina (C57BL/6J-rd le). *Invest Ophthalmol Vis Sci.* 1984;25:364–369.
41. Wang S, Villegas-Pérez MP, Vidal-Sanz M, Lund RD. Progressive optic axon dystrophy and vacuslar changes in rd mice. *Invest Ophthalmol Vis Sci.* 2000;41:537–545.

182

Development/Plasticity/Repair

Presynaptic Dystroglycan–Pikachurin Complex Regulates the Proper Synaptic Connection between Retinal Photoreceptor and Bipolar Cells

Yoshihiro Omori,[1,2,3]* Fumiyuki Araki,[1,2,4]* Taro Chaya,[1,2] Naoko Kajimura,[5] Shoichi Irie,[1,2] Koji Terada,[1] Yuki Muranishi,[1,2] Toshinori Tsujii,[1,2] Shinji Ueno,[6] Toshiyuki Koyasu,[6] Yasuhiro Tamaki,[4] Mineo Kondo,[7] Shiro Amano,[4] and Takahisa Furukawa[1,2]

[1]Department of Developmental Biology, Osaka Bioscience Institute, [2]Japan Science and Technology Agency, Core Research for Evolutional Science and Technology, and [3]Precursory Research for Embryonic Science and Technology, Osaka, 565-0874, Japan, [4]Department of Ophthalmology, University of Tokyo Graduate School of Medicine, Tokyo, 113-8655, Japan, [5]Research Center for Ultra-High Voltage Electron Microscopy, Osaka University, Osaka, 567-0047, Japan, [6]Department of Ophthalmology, Nagoya University Graduate School of Medicine, Nagoya, 466-8550, Japan, and [7]Department of Ophthalmology, Mie University Graduate School of Medicine, Mie, 514-8507, Japan

Dystroglycan (DG) is a key component of the dystrophin–glycoprotein complex (DGC) at the neuromuscular junction postsynapse. In the mouse retina, the DGC is localized at the presynapse of photoreceptor cells, however, the function of presynaptic DGC is poorly understood. Here, we developed and analyzed retinal photoreceptor-specific *DG* conditional knock-out (*DG* CKO) mice. We found that the *DG* CKO retina showed a reduced amplitude and a prolonged implicit time of the ERG b-wave. Electron microscopic analysis revealed that bipolar dendrite invagination into the photoreceptor terminus is perturbed in the *DG* CKO retina. In the *DG* CKO retina, pikachurin, a DG ligand in the retina, is markedly decreased at photoreceptor synapses. Interestingly, in the *Pikachurin*$^{-/-}$ retina, the DG signal at the ribbon synaptic terminus was severely reduced, suggesting that pikachurin is required for the presynaptic accumulation of DG at the photoreceptor synaptic terminus, and conversely DG is required for pikachurin accumulation. Furthermore, we found that overexpression of pikachurin induces formation and clustering of a DG–pikachurin complex on the cell surface. The Laminin G repeats of pikachurin, which are critical for its oligomerization and interaction with DG, were essential for the clustering of the DG–pikachurin complex as well. These results suggest that oligomerization of pikachurin and its interaction with DG causes DG assembly on the synapse surface of the photoreceptor synaptic terminals. Our results reveal that the presynaptic interaction of pikachurin with DG at photoreceptor terminals is essential for both the formation of proper photoreceptor ribbon synaptic structures and normal retinal electrophysiology.

Introduction

Dystrophin is an actin-binding cytoskeletal protein, and its mutation in humans causes various types of muscular dystrophy (MD) including Duchenne MD (DMD) and Becker MD (Hoffman and Kunkel, 1989). The dystrophin–glycoprotein complex (DGC) connects the extracellular matrix with the actin cytoskeleton in the neuromuscular junction (NMJ) and in non-muscle tissues including the brain and retina (Henry and Campbell, 1996). Dystroglycan (DG), a key component of the DGC, consists of an extracellular α-DG subunit and a transmembrane β-DG subunit. Several extracellular ligands for α-DG, including laminin, agrin, perlecan, and Pikachurin, have been reported (Ibraghimov-Beskrovnaya et al., 1992; Ervasti and Campbell, 1993; Gee et al., 1994; Peng et al., 1998; Sugita et al., 2001; Sato et al., 2008). These DG ligands commonly contain Laminin G repeats, and these domains physically interact with DG. For ligand binding of DG, glycosyltransferase-mediated glycosylation of DG is critical. Mutations of putative glycosyltransferase genes, including *Large*, *Fukutin*, *FKRP*, *PoMGnT1*, and *POMT1* and *POMT2*, have been identified in patients with congenital MD (Kobayashi et al., 1998; Brockington et al., 2001; Yoshida et al., 2001; Beltrán-Valero de Bernabé et al., 2002; Longman et al., 2003; van Reeuwijk et al., 2005).

Attenuation of ERGs is observed in both MD patients and their corresponding animal models (Haenggi and Fritschy,

Received Jan. 23, 2012; revised March 6, 2012; accepted March 15, 2012.

Author contributions: Y.O., F.A., Y.T., M.K., S.A., and T.F. designed research; Y.O., F.A., T.C., N.K., S.I., K.T., Y.M., T.T., S.U., T.K., and T.F. performed research; Y.O., F.A., T.C., N.K., S.I., and S.U. analyzed data; Y.O., F.A., T.C., N.K., S.U., and T.F. wrote the paper.

This work was supported by CREST and PRESTO from Japan Science and Technology Agency, a grant for Molecular Brain Science, Grants-in-Aid for Scientific Research on Priority Areas, and Grant-in-Aid for Scientific Research (B), Young Scientists (B); Specially Designated Research Promotion and Scientific Research on Innovative Areas "Intracellular Logistics" from the Ministry of Education, Culture, Sports and Technology of Japan; The Takeda Science Foundation; The Uehara Memorial Foundation; Novartis Foundation; Mochida Memorial Foundation for Medical and Pharmaceutical Research and The Naito Foundation; Senri Life Science Foundation; Kato Memorial Bioscience Foundation; Daiichi-Sankyo Foundation of Life Science; Japanese Retinitis Pigmentosa Society Foundation; and Research Foundation for Opto-Science and Technology. We thank Dr. Kevin Campbell for the DG-flox mouse, and M. Kadowaki, A. Tani, A. Ishimaru, Y. Saioka, H. Abe, and S. Kennedy for technical assistance.

*Y.O. and F.A. contributed equally to this work.

The authors declare no competing financial interests.

Correspondence should be addressed to Takahisa Furukawa, Department of Developmental Biology, Osaka Bioscience Institute, 6-2-4 Furuedai, Suita, Osaka, 565-0874, Japan. E-mail: furukawa@obi.or.jp.

DOI:10.1523/JNEUROSCI.0322-12.2012

 0270-6474/12/326126-12$15.00/0

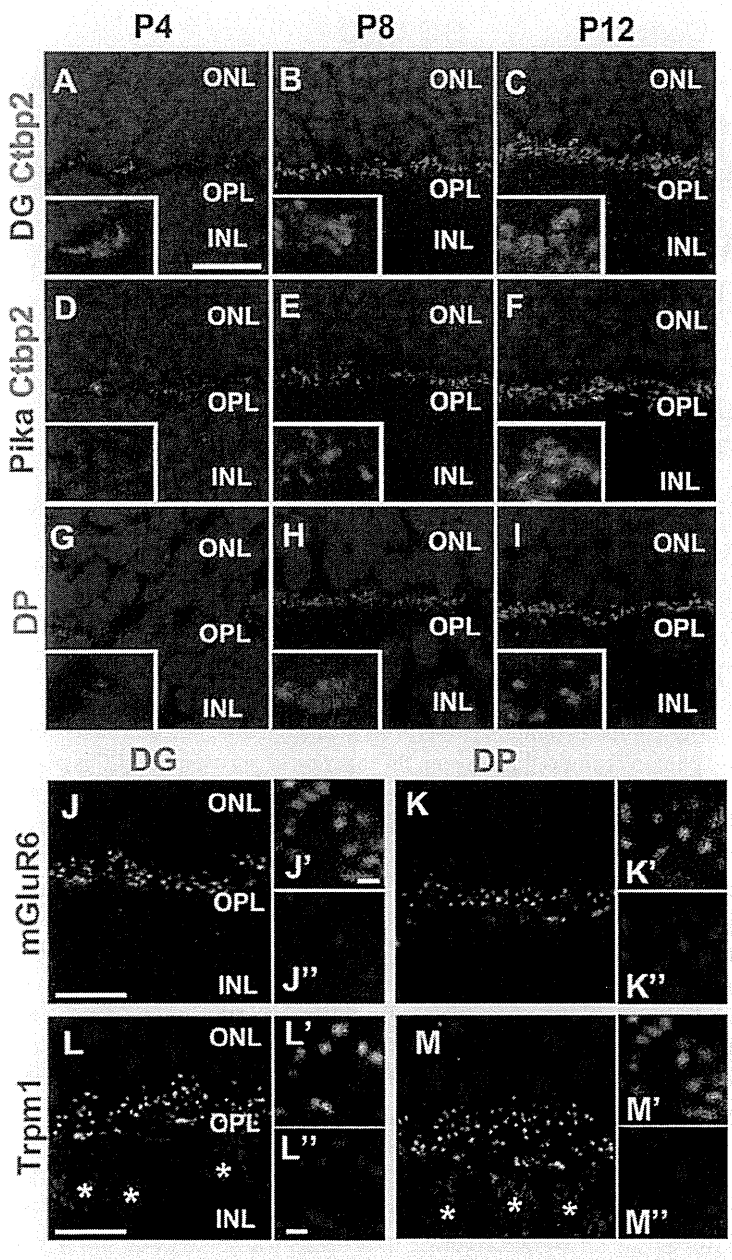

Figure 1. Dystrophin, DG, and Pikachurin are localized at photoreceptor synaptic terminals in the OPL of the developing mouse retina. Retinal sections isolated from P4 (*A*, *D*, *G*), P8 (*B*, *E*, *H*), and P12 (*C*, *F*, *I*) wild-type mice were stained with antibodies against DG (red in *A–C*), Pikachurin (red in *D–F*), dystrophin (green in *G–I*), and CtBP2 (a synaptic ribbon marker, green in *A–F*). Higher-magnification views of photoreceptor synapses were shown in the insets. Nuclei were stained with DAPI (blue). DG, Pikachurin, and dystrophin signals were observed in the OPL where photoreceptors form synapses with horizontal and bipolar cells. Retinal sections of adult mice were stained with antibodies against DG (green in *J–J''*, *L–L''*), dystrophin (green in *K–K''*, *M–M''*), mGluR6 (red in *J–K''*), or TRPM1 (red in *L–M''*). Asterisks indicate TRPM1-positive bipolar cells in the INL (*L*, *M*). DG and dystrophin signals at photoreceptor synapses were colocalized with mGluR6- and TRPM1-positive bipolar dendritic terminals in the OPL. DG, Pikachurin, and dystrophin signal puncta at photoreceptor ribbon synapses become visible in the OPL after P8. Scale bars: *A*, *J*, *L*, 10 μm; *J'*, *L''*, 1 μm.

2006). Reduction of the amplitude of the b-wave response is observed in 80% of DMD patients (Cibis et al., 1993; Pillers et al., 1993; Fitzgerald et al., 1994; D'Souza et al., 1995). Reduced amplitude and prolonged implicit time of the b-wave, a response of positive polarity originating primarily from the ON-bipolar cells, have been observed in ERGs from various types of MD model mice (Pillers et al., 1995; Lee et al., 2005; Liu et al., 2006). In the retina, DG is found in Müller glial endfeet abutting the inner limiting membrane (ILM) and perivascular glial endfeet as well as photoreceptor synapses in the retinal OPL (Schmitz and Drenckhahn, 1997b; Ueda et al., 2000; Blank et al., 2002). Photoreceptor axonal terminals form ribbon synapses in the OPL, which connect photoreceptor presynapses with the dendritic terminal of both bipolar cells and horizontal cells (tom Dieck and Brandstätter, 2006). We previously reported that an extracellular matrix protein, Pikachurin, is essential for the proper formation of ribbon synaptic structures (Sato et al., 2008). *Pikachurin*$^{-/-}$ mice showed a reduced amplitude and prolonged implicit time of the b-wave similar to other mutant mice with perturbed DGC formation. Pikachurin physically interacts with DG, and proper glycosylation of DG is required for its interaction with Pikachurin (Sato et al., 2008; Kanagawa et al., 2010). It was reported that the loss of DG in Müller glial cells causes ERG abnormality (Satz et al., 2009). However, the functional role of presynaptic DG in photoreceptor cells remains unclear.

Here, we report the retinal phenotypes of photoreceptor-specific *DG* conditional knock-out (*DG* CKO) mice. Our results show that presynaptic DG–Pikachurin complex is essential for the proper formation of the photoreceptor ribbon synapse and normal retinal electrophysiology.

Materials and Methods

Generation of the DG CKO mouse. We mated a *DG*^{flox} (Moore et al., 2002) mouse line with a *Crx-Cre* transgenic mouse line, which expresses Cre recombinase under the control of the 2 kb *Crx* promoter (Furukawa et al., 2002). We confirmed Cre-mediated recombination of a LacZ reporter transgene of the *CAG-CAT-Z* Cre monitor mice in the developing and mature photoreceptor layer, and also confirmed the cell fate change of photoreceptor precursors by mating with the *Otx2*^{flox} mice as previously reported (Nishida et al., 2003). All procedures conformed to the ARVO (Association for Research in Vision and Ophthalmology) Statement for the Use of Animals in Ophthalmic and Vision Research, and were approved by the Institutional Safety Committee on Recombinant DNA Experiments and the Animal Research Committee of Osaka Bioscience Institute. Mice were housed in a temperature-controlled room with a 12 h light/dark cycle. Fresh water and rodent diet were available at all times.

Immunohistochemistry. Mouse eyes of either sex were fixed in 4% paraformaldehyde in PBS for 30 s or 5 min, embedded in TissueTek OCT compound 4583 (Sakura Finetek), frozen, and sectioned. Frozen 20 μm sections on slides were dried for 30 min at room temperature, rehydrated in PBS for 5 min, incubated with blocking solution (5% normal goat serum and 0.5% Triton X-100 in PBS) for 1 h, and then with primary antibodies for 4 h at room temperature. Slides were washed with PBS three times for 10 min each time and incubated with secondary antibodies for 2 h at room temperature. The specimens were observed under a

laser confocal microscope (LSM510, Carl Zeiss). We used the following primary antibodies: mouse monoclonal antibodies specific to CtBP2 (C-terminal binding protein 2) (1:1000, BD Biosciences), dystrophin (1:300, Millipore Bioscience Research Reagents MAB1692), and PKC (1:1000, Sigma P5704); rabbit polyclonal antibodies to β-dystroglycan H-242 (1:300, Santa Cruz Biotechnology), TRPM1(1:500) (Koike et al., 2010) and Pikachurin (1:500, Wako Chemicals 011-22631) (Sato et al., 2008); and a guinea pig polyclonal antibody against mGluR6 (1:3000) (Koike et al., 2010). We used Cy3-conjugated secondary antibodies (1:400, Jackson ImmunoResearch Laboratories) and Alexa Fluor 488-conjugated secondary antibodies (1:400, Sigma).

ERG recordings. Electroretinographic recordings were performed as described previously (Chen et al., 2004). In brief, 2- to 6-month-old mice of either sex were dark-adapted overnight, and then anesthetized with an intramuscular injection of 70 mg/kg ketamine and 14 mg/kg xylazine. ERGs were recorded with a gold-wire loop electrode placed on the anesthetized cornea. The mice were placed in a Ganzfeld bowl and stimulated with stroboscopic stimuli of 1.0 log cd-s/m^2 (photopic units) maximum intensity. Four levels of stimulus intensities ranging from −5.0 to 1.0 log cd-s/m^2 were used for the scotopic ERG recordings, and four levels of stimuli ranging from −0.5 to 1.0 log cd-s/m^2 were used for the photopic ERGs. The photopic ERGs were recorded on a rod-suppressing white background of 1.3 log cd-s/m^2.

Electron tomography. For observation by transmission electron microscope, 500-nm-thick sections of the 2-month-old mouse retinas of either sex were cut with a diamond knife (Nanotome) using a Reichert Ultracut E ultramicrotome (Leica), and mounted on Formvar-coated 50 mesh square grids. Sections were stained as described previously (Takaoka et al., 2008). Colloidal gold beads (20 nm; BB International), used as fiducial markers for alignment, were applied to the section surface. Sections were stabilized with a layer of evaporated carbon. Tomographic data were recorded automatically using an H-9500SD (Hitachi Co.) transmission electron microscope operated at an acceleration voltage of 300 kV. Data were recorded at a microscopic magnification of 15,000× (at 1.23 nm/pixel) from −60° to +60° at 2° intervals around a single axis and collected with a 2048 × 2048 CCD camera F224HD (Tietz Video and Imaging Processing Systems). For each tomography experiment, 5 and 15 different rod terminals from two wild-type and three mutant retinas, respectively, were observed. Image processing, including alignment and 3D reconstruction, was performed with the IMOD package as described previously (Kremer et al., 1996).

Cell culture and transfection. HEK293 cells were grown in DMEM (Sigma) with 10% fetal calf serum and 2 mg/L L-glutamine. Transfection was performed using Lipofectamine-LTX (Invitrogen) according to the manufacturer's instructions. At 72 h after transfection, cells were washed with PBS, fixed with 4% paraformaldehyde in PBS for 3 min at room temperature, and subsequently incubated with blocking solution for 30 min. Cells were immunostained with a primary antibody in the blocking solution for 4 h at room temperature, and subsequently incubated with the secondary antibody solution for 2 h at room temperature.

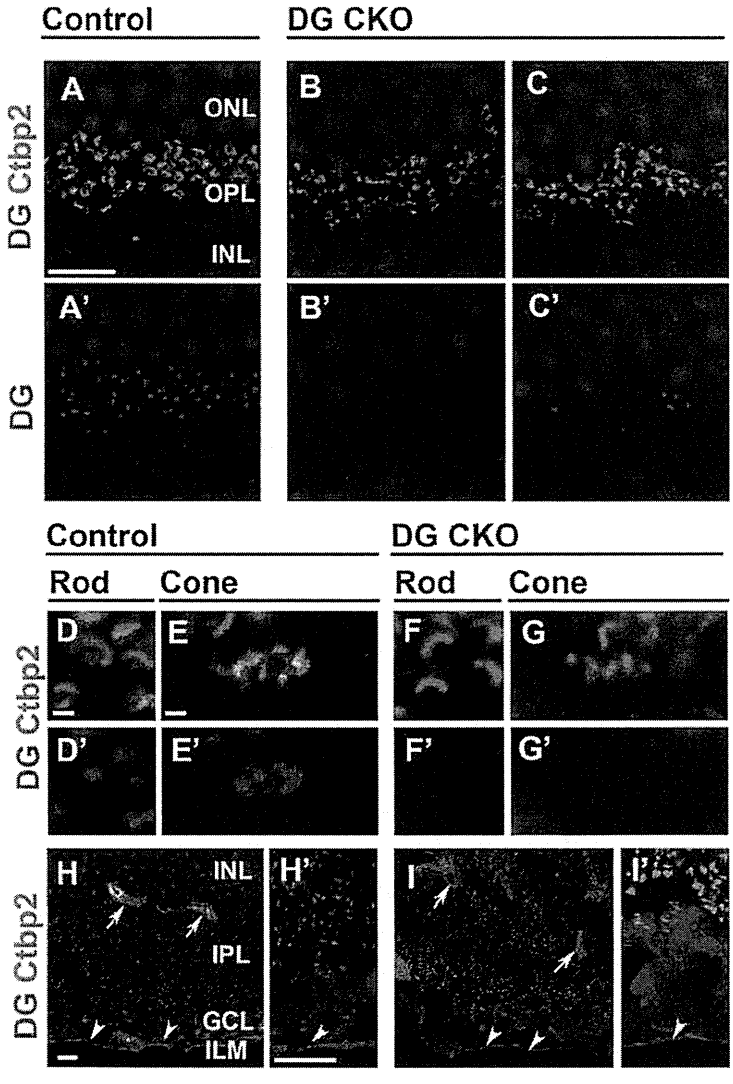

Figure 2. DG in photoreceptor ribbon synapses is depleted in the *DG* CKO retinas. Immunohistochemical analysis of DG in the control and *DG* CKO retinas. Retinal sections from control (*A*, *A'*, *D*, *D'*, *E*, *E'*, *H*, *H'*) and *DG* CKO (*B*, *B'*, *C*, *C'*, *F*, *F'*, *G*, *G'*, *I*, *I'*) mice were stained with antibodies against DG (red) and CtBP2 (green), a synaptic ribbon marker in the ribbon synapse of the OPL. Nuclei were stained with DAPI (blue). Higher-magnification views of rod (*D*, *D'*, *F*, *F'*) and cone (*E*, *E'*, *G*, *G'*) photoreceptor ribbon synapses are shown. Higher-magnification views of *H* and *I* are shown in *H'* and *I'*, respectively. In the control retina, DG signal is observed at the OPL in photoreceptors (*A*), blood vessels (arrow in *H*), and the ILM (*H*, arrowheads). In the *DG* CKO retina, DG signal in the OPL is severely depleted (*B*, *C*), whereas it remains in blood vessels (arrow in *I*) and the ILM (arrowheads in *I*, *I'*). Scale bars: *A*, *H*, *H'*, 10 μm; *D*, *E*, 1 μm. IPL, inner plexiform layer.

Western blot analysis. Transfected HEK293 cells were washed by PBS twice and lysed in a SDS-sample buffer. Western blot analysis was performed using a semidry transfer cell (iBlot system, Invitrogen) with iBlot Gel Transfer Stack PVDF (Invitrogen). Signals were detected using Can Get Signal (Toyobo) and ECL Plus Western Blotting Detection System (GE Healthcare Life Sciences).

Results

Dystrophin, DG, and Pikachurin are colocalized at retinal photoreceptor synaptic terminals

To investigate the subcellular localization of the DGC components at the synapses of developing retinal photoreceptors, we immunostained Pikachurin, DG, and dystrophin in the OPL where the photoreceptor, bipolar, and horizontal cell processes form ribbon synapses. Retinal sections from P4, P8, and P12 WT mice were stained with antibodies against Pikachurin, DG, dystrophin, and a synaptic ribbon marker, CtBP2 (Fig. 1*A–I*). At P4,